Experimental Neurology 313 (2019) 109–123

Contents lists available at ScienceDirect

Experimental Neurology

journal homepage: www.elsevier.com/locate/yexnr

Research Paper

Chronic stress increases pain sensitivity via activation of the rACC–BLA pathway in rats

Ling-Yu Liu[a], Rui-Ling Zhang[b], Lin Chen[a], Hong-Yan Zhao[a], Jie Cai[a,c], Jia-Kang Wang[e], Da-Qing Guo[e], Yan-Jun Cui[d,*], Guo-Gang Xing[a,b,c,*]

[a] Department of Neurobiology, School of Basic Medical Sciences and Neuroscience Research Institute, Peking University, Beijing 100083, China
[b] The Second Affiliated Hospital of Xinxiang Medical University, Henan, Xinxiang 453002, China
[c] Key Laboratory for Neuroscience, Ministry of Education/National Health Commission, Beijing 100083, China
[d] Department of Internal Medicine, Peking University Hospital, Beijing 100871, China
[e] Key Laboratory for NeuroInformation of Ministry of Education, School of Life Science and Technology, University of Electronic Science and Technology of China, Chengdu 610054, China

ARTICLE INFO

Keywords:
Chronic forced swim stress
Stress–induced hyperalgesia
Rostal anterior cingulate cortex
Amygdala
Field potential power
Local field potential
Rat

ABSTRACT

Exposure to chronic stress can produce maladaptive neurobiological changes in pathways associated with pain processing, which may cause stress–induced hyperalgesia (SIH). However, the underlying mechanisms still remain largely unknown. In previous studies, we have reported that the amygdala is involved in chronic forced swim (FS) stress–induced depressive-like behaviors and the exacerbation of neuropathic pain in rats, of which, the basolateral amygdala (BLA) and the central nucleus of the amygdala (CeA) are shown to play important roles in the integration of affective and sensory information including nociception. Here, using in vivo multichannel recording from rostal anterior cingulate cortex (rACC) and BLA, we found that chronic FS stress (CFSS) could increase the pain sensitivity of rats in response to low intensity innoxious stimuli (LIS) and high intensity noxious stimuli (HNS) imposed upon the hindpaw, validating the occurrence of SIH in stressed rats. Moreover, we discovered that CFSS not only induced an increased activity of rACC neuronal population but also produced an augmented field potential power (FPP) of rACC local field potential (LFP), especially in low frequency theta band as well as in high frequency low gamma band ranges, both at the baseline state and under LIS and HNS conditions. In addition, by using a cross-correlation method and a partial directed coherence (PDC) algorithm to analyze the LFP oscillating activity in rACC and BLA, we demonstrated that CFSS could substantially promote the synchronization between rACC and BLA regions, and also enhanced the neural information flow from rACC to BLA. We conclude that exposure of chronic FS stress to rats could result in an increased activity of rACC neuronal population and promote the functional connectivity and the synchronization between rACC and BLA regions, and also enhance the pain–related neural information flow from rACC to BLA, which likely underlie the pathogenesis of SIH.

1. Introduction

Chronic stress–induced depression disorder can increase the suffering of patients and their family members (Yankelevitch-Yahav et al., 2015), which is a very important health issue. Stress–induced hyperalgesia (SIH) (Jennings et al., 2014), as well as the comorbidity of pain with chronic stress–related depression disorder, represent a series of significant clinical challenges in modern society (Gerrits et al., 2014; Li, 2015). Depressive patients often experience greater severe pain (Akechi et al., 2012). Besides, anxiety and depression-like behaviors have also been observed to be significantly increased in rats with neuropathic pain (Goncalves et al., 2008). Many patients with chronic pain also

Abbreviations: ANOVA, analysis of variance; BLA, basolateral amygdala; CeA, central nucleus of the amygdala; CFSS, chronic forced swim stress; dACC, dorsal anterior cingulate cortex; DC, direct Current; FFT, fast Fourier transformation; FPP, field potential power; FS, forced swim; HNS, high intensity noxious stimuli; i.m., intramuscular injection; i.p., intraperitoneal injection; LA/BLA, lateral/basolateral amygdala; LFP, local field potential; LIS, low intensity innoxious stimuli; PAG, periaqueductal gray; PB, parabrachial nuclei; PDC, partial directed coherence; rACC, rostal anterior cingulate cortex; SIH, stress–induced hyperalgesia.

* Corresponding authors at: Department of Neurobiology, School of Basic Medical Sciences and Neuroscience Research Institute, Peking University, Beijing 100083, China (G-G Xing); Department of Internal Medicine, Peking University Hospital, Beijing 100871, China (Y-J Cui).

E-mail addresses: cyj@pku.edu.cn (Y.-J. Cui), ggxing@bjmu.edu.cn (G.-G. Xing).

https://doi.org/10.1016/j.expneurol.2018.12.009
Received 22 October 2018; Accepted 21 December 2018
Available online 23 December 2018
0014-4886/

seem to have clear symptoms relating to anxiety and depression. In clinical practice, chronic pain is also associated with negative emotional reactions and cognitive impairment (Jensen et al., 2012). Previously, we have reported that the amygdala is involved in chronic forced swim (FS) stress–induced depressive-like behaviors and the exacerbation of neuropathic pain in rats (Chen et al., 2018a; Li et al., 2017), of which, the basolateral amygdala (BLA) and the central nucleus of the amygdala (CeA) are shown to play important roles in the integration of affective and sensory information including nociception (Li et al., 2017; Padival et al., 2013).

Chronic stress causes morphological and functional changes in many brain regions. Multiple cortical and subcortical areas are found to play crucial roles in the modulation of chronic stress–relevant negative emotion, depression and chronic pain. The anterior cingulate cortex (ACC) is a critical hub for nociceptive perception and pain–related anxiety (Guo et al., 2018), which can be divided into a cognitive region (dorsal ACC, dACC) and an affective region (rostral ACC, rACC) (Shinozaki et al., 2016). The rACC closely connects with the amygdala (Matyas et al., 2014), periaqueductal gray (PAG), hypothalamus, hippocampus, and orbitofrontal cortex, thereby participating in autonomic nervous activity, endocrine activity, the motivation information evaluation, and the emotional responses. Functionally, the amygdala receives both multi-sensory information from the superior cortical region via the lateral/basolateral amygdala (LA/BLA) and the direct projections of nociceptive information from the parabrachial nuclei (PB) (Bianchi et al., 1998; Strobel et al., 2014). Highly integrated stress-affective–related information is then transmitted to the CeA, an output nucleus for the major functions of the amygdala, to modulate the pain–related behaviors. The BLA has, important roles in the modulation of neuropathic pain, including the neural circuit that processes the affective-motivational component of pain (Seno et al., 2018). Also, the BLA is highly associated with a variety of brain functions and diseases, such as cognitive and emotional functions (Sharp, 2017), and the hyperexcitability of BLA neurons is involved in the pathogenesis of SIH. Direct neuronal projections from ACC to BLA play a critical role in modulation emotional functions such as fear learning (Allsop et al., 2018; Jhang et al., 2016). Therefore, chronic forced swim (FS) stress not only leads to the hyperactivation of rACC neurons (Clauss et al., 2014), but also increases the interaction between rACC and amygdala (Yoshimura et al., 2010). Theoretically, the alterations of rACC neurons activity may consequently impact the activity of BLA neurons in SIH state.

Based on the above evidence, we hypothesized that the chronic stress–induced augmentation of pain sensitivity may depend upon the activation of the rACC–BLA pathway, that is, the increased excitability of rACC neurons and the enhanced information flow from rACC to BLA. In this study, by using an in vivo multiple-channel recording technique in free-moving rats, we investigated whether exposure of CFSS to rats would exacerbate the pain sensitivity in response to the innoxious and noxious stimuli imposed to the hindpaw. Furthermore, we examined whether the increased activity of rACC neuronal population and the power spectra activities of rACC local field potential (LFP), as well as the enhanced pain–related neural information flow from rACC to BLA, would underlie the pathogenesis of SIH.

2. Materials and methods

2.1. Animals

Male Sprague-Dawley rats, weighing 300-350 g at the beginning of the experiment, were provided by the Department of Experimental Animals Sciences, Peking University Health Science Center. The rats were housed in separated cages with free access to food and water, and maintained in a temperature (20–22 °C), humidity (50–55%) and illumination (12: 12-h light: dark cycle) controlled vivarium. All procedures were approved by the Animal Care and Use Committee of Peking University.

2.2. Chronic forced swim stress (CFSS) procedure

In this study, chronic forced swim (FS) was chosen as a stressor, and carried out according to the procedure as previously described (Li et al., 2017; Shishkina et al., 2015). Briefly, the rats were placed in a glass cylinder (45 cm high, 20 cm in diameter) filled with ice water (0 ± 2 °C) up to a height of 30 cm. The FS procedure was conducted to rats individually once per day in 15-min sessions, continued for 7 consecutive days. According to the methods described elsewhere (Suarez-Roca et al., 2008), control rats were subjected to a sham swimming (sham FS) sessions by allowing them to wade in the cylinder that contained only 2–4 cm of warm water at 24–26 °C. Here we used sham FS animals rather than naïve animals as control for the reason to exclude the factor of habituation for rats to the water (Bogdanova et al., 2013). Rats were allowed to dry in a warm environment (30–33 °C) after swimming. The water was changed and the container was thoroughly cleaned for each rat. Electrophysiological activities and behavioral tests were recorded respectively before and after the FS procedure.

2.3. In vivo multi-channel recording

2.3.1. Surgery

Prior to the implantation of microelectrode array, initial anaesthesia was administered by pentobarbital sodium injection (50 mg/kg, *i.p.*). Supplementary doses (1/3 of the original dose) of pentobarbital sodium were given to maintain a proper anesthetic depth during surgery. Rats were mounted on a stereotaxic apparatus (Reward Life Science Technology Co. Ltd., Shenzhen), and an array of eight nickel chromium alloy wire PEG 2000-insulated microwires (14 µm in diameter, arranged in a 4 × 2 configuration, 250 µm spacing between each microwire, STABLOHM 675, California Fine Wire Company, USA) were slowly lowered into the right rACC (0 to 2.0 mm rostral to the bregma, 0 to 1.2 mm lateral from midline, and depth of 1.5 mm) and the right BLA (1.6 to 3.4 mm posterior to the bregma, 4.4 to 5.5 mm lateral from midline, and 6.8 mm ventral relative to the dura), according to the Rats Atlas of Paxinos and Watson (Paxinos and Watson, 2005). Six stainless steel screws were driven into the skull to serve as anchors for cementing the microwires in place after implantation. Rats were received penicillin injection (16,000 IU, *i.m.*) before surgery to prevent infection, and after surgery, they were allowed to recover for one week before recording sessions commenced.

2.3.2. Electrophysiological recording

Rats were placed in a transparent plastic chamber (40 × 40 × 30 cm, with a 2 × 8 mm stainless grid plate) in a quiet room at 22 ± 1 °C and allowed to move freely throughout the recording period. Electrophysiological signals were recorded after the animals adapted to the experimental environment. Data were collected at baseline (before stress) and on day 1 after a 7 consecutive-days stress (after stress). Multi-unit neuronal activity and broadband local field potential (LFP) signals were recorded simultaneously from the rACC and BLA with a Plexon multi-channel recording system (Plexon, Hong Kong). Neuronal spike signals were collected through the implanted microwire assemblies that were connected to a preamplifier via a head stage plug and a light-weight cable, and the ground wire was used as a reference. The outputs of the preamplifier were filtered (0.5 and 5 kHz, 6 dB cut-off) and sent to a multichannel spike-sorting device (Plexon, Hong Kong) for online signal processing. In our experiments, the spontaneous activity of rACC and BLA neurons were taken from a 400-s time-window as sampling. Spike train activity was analyzed by the software of NeuroExplorer (Plexon, Hong Kong). Waveform capture and frequency distribution histogram were used to verify the online classification of a single unit. Different waveforms were individually distinguished by setting multiple time-voltage windows using Offline-Sorter software (Plexon, Hong Kong). The time stamps of these waveforms were then stored on a personal computer for off-line analysis. In our present study, the spontaneous- and the laser stimuli-evoked activities of rACC and BLA neurons, induced by the low intensity innoxious stimuli (LIS) and the high intensity noxious stimuli (HNS) to rats, were recorded before and after stress exposure, respectively. The evoked activities of rACC and BLA neurons were sampled and analyzed during a time-frame from the 2 s before laser stimuli to the 2 s after laser stimuli. Each recording session contained 10 LIS trials and 10 HNS trials at random, with no less than 120 s inter-stimulus interval to avoid hyperalgesia.

Meanwhile, LFP signals were recorded from the right rACC and BLA by microwire arrays with a multi-channel data acquisition system (Plexon, Hong Kong). The LFP signals were transmitted from the headstage assemblies to the preamplifier via a light-weight cable. LFPs were collected at a sampling frequency of 10 kHz, amplified (300 ×), and band-pass filtered (0.3–500 Hz). LFP signals were filtered into five frequency bands: theta (4–8 Hz), alpha (9–12 Hz), beta (13–30 Hz), low gamma (31–70 Hz), and high gamma (71–100 Hz), in which the theta, alpha and beta bands belong to the low frequency band (4–30 Hz), while the low gamma and high gamma bands belong to the high frequency band (31–100 Hz). These five frequency bands, as well as the broadband (4–100 Hz) LFP signals, were then analyzed via a Hilbert transform.

2.3.3. Data analysis

The neuronal firing rate was quantified for each neuron using analysis program NeuroExplorer (Plexon, Hong Kong) to construct rate histogram with a time-frame from the beginning to 5 min after stress in different groups. The bin sizes were 1 s and 50 milliseconds for the computation of baseline and LIS/HNS-evoked firing histogram, respectively. Bin counts for each trial were calculated using the analysis program NeuroExplorer (Plexon, Hong Kong) and the results were exported to Matlab (The MathWorks, Inc.) in spreadsheet form. The firing rates for all neurons were normalized and arranged into a spreadsheet for further statistical analysis. Field potential power (FPP) was analyzed with the NeuroExplorer (Plexon, Hong Kong) and Matlab toolbox Chronux (*http://chronux.org*). Local field potential (LFP) data were resampled at 1 kHz and analyses were performed separately for each 400-s epoch of recording to baseline LFP, or for each 4-s (from the 2 s before laser stimuli to the 2 s after laser stimuli) epoch of recording to LIS/HNS-evoked LFP. Then the time-varying power spectra was calculated by fast Fourier transformation (FFT). Power spectral analysis was performed to calculate FPP.

2.4. Behavioral test

In all experiments, electrophysiological signals and the video recording for the animals' behaviors were simultaneously recorded. Cineplex Studio software was used to synchronize videos to record the behaviors of rats. In our experiments, the spontaneous- and the laser stimuli-evoked activity of rACC and BLA neurons, induced by the low intensity innoxious stimuli (LIS) and the high intensity noxious stimuli (HNS) to rats, were recorded before and after stress exposure, respectively. The laser beam (10.6 mm in wavelength, 2.5 mm in diameter and 10 ms in pulse width), that imposed on the left hindpaw of the rat through the multi-row holes at the bottom of the plastic chamber, was delivered by an CO_2 laser therapeutic machine (DIMEI-300, Changchun Optics Medical Apparatus Co. Ltd., China). Nociceptive behaviors were identified by the immediate paw withdrawal response to the imposed laser stimuli. The power of HNS was set as 120% paw withdrawal threshold (approximately 8 to 12 milliwatts), while the power of LIS was set as 80% paw withdrawal threshold (usually below 4 milliwatts). Nociceptive behavioral test was simultaneously recorded with each electrophysiological recording session.

2.5. Histology

After the termination of the experiment, rats were deeply anesthetized with pentobarbital sodium and the tip positions of the electrodes were identified by a 2 mA, 10 s DC current (anode current) through the electrodes to produce thermally lesion of the near area tissue. The animals were then sacrificed and perfused with 0.9% saline followed by 4% paraformaldehyde. After fixing in paraformaldehyde at 4 °C overnight, the brains were transferred to a 20% sucrose solution in saline for cryoprotection. Coronal sections of 30 μm were cut on a microtome, mounted on charged slides, and stained with neutral red dye for 10–15 min. Recording sites were determined under a light microscope (supplementary data, Fig. S1). Data of those sites deflecting from the target area were excluded from analysis.

2.6. Statistical analysis

Data statistical analyses and figure plotting were performed by software of Matlab 2015a (The MathWorks, Inc.) and GraphPad Prism 7.0 (GraphPad Software, Inc., La Jolla, USA). All data were expressed as mean ± standard error of the mean. A two-tailed unpaired *t*-test was used for the comparison of the mean values between two groups. Two-way analysis of variance (ANOVA) followed by Bonferroni or Tukey post-hoc test was used for multiple comparison. Differences with $P < 0.05$ were considered statistically significant.

3. Results

3.1. Chronic forced swim stress increases the pain sensitivity of rats in response to low intensity innoxious stimuli (LIS) and high intensity noxious stimuli (HNS)

In order to explore the effects of chronic forced swim stress (CFSS) on nociceptive behaviors in rats, we examined the pain sensitivity induced by innoxious- and noxious-laser stimuli imposed upon the hindpaw, respectively. The experimental procedure is shown in Fig. 1A. The behavioral results revealed that in CFSS-treated rats, the paw withdrawal ratio of rats was increased significantly in response to both low intensity innoxious stimuli (LIS) (32.5 ± 4.8% after CFSS vs. 5.0 ± 5.0% before CFSS, $F_{1,12} = 3.56$, P = 0.0065, Fig. 1B) and high intensity noxious stimuli (HNS) (97.5 ± 2.5% after CFSS vs. 50.0 ± 15.8% before CFSS, $F_{1,14} = 0.31$, P = 0.0365, Fig. 1C) (two-way ANOVA, n = 4–5 rats per group). And also, the paw withdrawal ratio of rats to the LIS was substantially increased (32.5 ± 4.8% after CFSS vs. 12.5 ± 7.5% after sham CFSS, $F_{1,12} = 3.56$, P = 0.0411, Fig. 1B) in CFSS-treated rats compared with the sham CFSS-treated rats (two-way ANOVA, n = 4 rats per group). However, in sham CFSS-treated rats, no significant alteration was observed on the paw withdrawal ratio either in response to LIS (12.5 ± 7.5% after sham stress vs. 5.0 ± 2.9% before sham stress, $F_{1,12} = 3.56$, P = 0.6741) or to HNS (87.5 ± 6.3% after sham stress vs. 54.0 ± 14.7% before sham stress, $F_{1,14} = 0.31$, P = 0.1554) (two-way ANOVA, n = 4–5 rats per group). These results indicated that exposure of CFSS to rats could induced an increased pain sensitivity, that is, stress–induced hyperalgesia (SIH) as observed in patients.

3.2. Chronic forced swim stress increases the baseline activity of rACC neurons in rats

Long-term negative events exposure, such as CFSS, can change the excitability of cortical neurons. In order to determine the effect of CFSS on the baseline activity of rACC neurons, we first examined the spontaneous activity of rACC neurons in rats exposed to CFSS or sham CFSS using in vivo multichannel recording technique. A total of 132 rACC neurons were recorded, including 73 neurons in 6 CFSS-treated rats, and 59 neurons in 4 sham CFSS-treated rats. Representative baseline

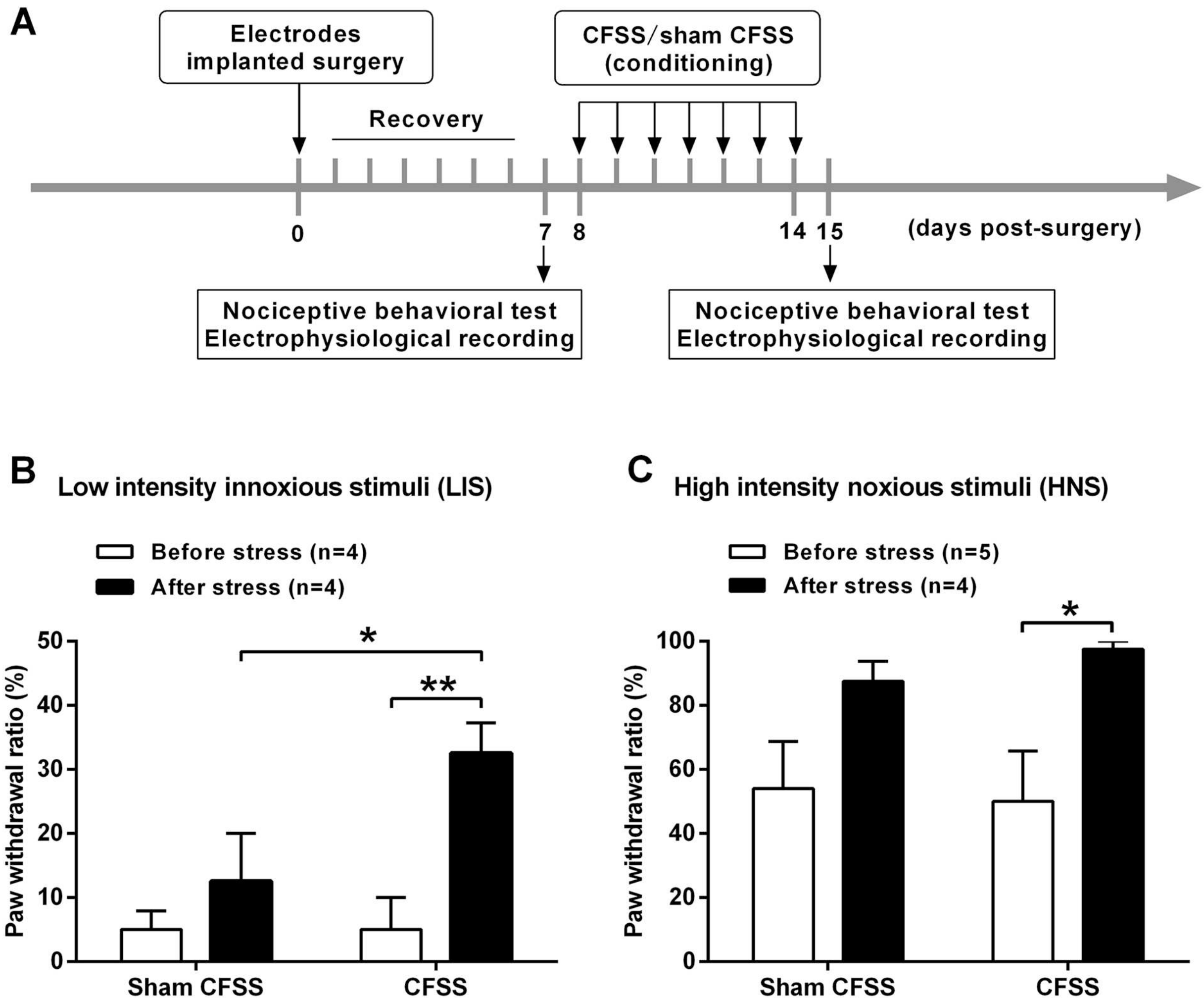

Fig. 1. Effects of chronic forced swim stress (CFSS) on the pain sensitivity of rats in response to innoxious- and noxious-laser stimuli imposed upon the hindpaw. (A): Schematic representation of the experimental procedure. (B, C): Effects of CFSS on the paw withdrawal ratio of rats in response to low intensity innoxious stimuli (LIS) (B) and high intensity noxious stimuli (HNS) (C). Note that CFSS induces a significant increase in the paw withdrawal ratio of rats in response to both LIS and HNS. *$P < 0.05$ or **$P < 0.01$, two-way ANOVA followed by Bonferroni post-hoc test, n = 4–5 rats per group.

firing activity of rACC neurons in rats exposed to CFSS or sham CFSS are shown in Fig. 2A to D. The statistical results disclosed that the mean spontaneous firing rate of rACC neurons (during a 400-s time-window of sampling) was significantly increased in rats after exposure of CFSS (in spikes/s, 5.45 ± 0.36 after CFSS vs. 3.52 ± 0.22 before CFSS, $F_{1,247}$ = 17.51, P < 0.0001, two-way ANOVA, Fig. 2C, D and E). In contrast, no significant alteration was observed on the mean spontaneous firing rate of rACC neurons in rats subjected to sham CFSS (in spikes/s, 3.10 ± 0.16 after sham CFSS vs. 3.42 ± 0.25 before sham CFSS, $F_{1,247}$ = 17.51, P = 0.8542, two-way ANOVA, Fig. 2A, B and E). Moreover, the mean spontaneous firing rate of rACC neurons also was prominently increased in CFSS-treated rats compared with the sham CFSS-treated rats after exposure of stress (in spikes/s, 5.45 ± 0.36 CFSS vs. 3.10 ± 0.16 sham CFSS, $F_{1,247}$ = 17.51, P < 0.0001, two-way ANOVA, Fig. 2E). In addition, after exposure of stress, the normalized firing rate of rACC neurons relative to the mean baseline activity (i.e. pre-stress) was 154.6 ± 10.2% of pre-stress in CFSS-treated rats and 90.7 ± 4.7% of pre-stress in sham CFSS-treated rats, respectively (t_{117} = 5.21, P < 0.0001, unpaired two-tailed t-test, Fig. 2F). These data suggested that exposure of CFSS to rats could enhance the baseline activity of rACC neurons, that is, induced a sensitization of rACC neurons.

3.3. Chronic forced swim stress increases the rACC neuron activity induced by low intensity innoxious stimuli (LIS) and high intensity noxious stimuli (HNS) to rats

Next, we examined the LIS- and HNS-evoked firing rate of rACC neurons before and after exposure of stress to rats. The evoked firing rate of rACC neurons was sampled and analyzed during a time-window from the 2 s before laser stimuli to the 2 s after laser stimuli. Representative LIS- and HNS-evoked firing activity of rACC neurons in rats exposed to CFSS or sham CFSS are shown in Fig. 3A and D, respectively. The statistical results uncovered that in CFSS-treated rats, both LIS and HNS induced a substantially increase in the laser-evoked firing rate of rACC neurons after stress exposure. For example, the LIS-evoked firing rate (in spikes/s) of rACC neurons was increased from 4.26 ± 0.32 before CFSS to 10.07 ± 0.46 after CFSS ($F_{1,161}$ = 61.64, P < 0.0001, two-way ANOVA, Fig. 3B), and the HNS-evoked firing rate was increased from 8.58 ± 0.39 before CFSS to 22.86 ± 0.51 after CFSS ($F_{1,166}$ = 239.6, P < 0.0001, two-way ANOVA, Fig. 3E), respectively. However, as that in sham CFSS-treated rats, the laser-evoked firing rate (in spikes/s) of rACC neurons was not significantly altered either after application of LIS (5.00 ± 0.42 before sham CFSS vs. 4.51 ± 0.31 after sham CFSS, $F_{1,161}$ = 61.64, P = 0.8454, two-way ANOVA, Fig. 3B) or after application of HNS (7.21 ± 0.39 before sham CFSS vs. 7.78 ± 0.44 after sham CFSS, $F_{1,166}$ = 239.6, P = 0.7803,

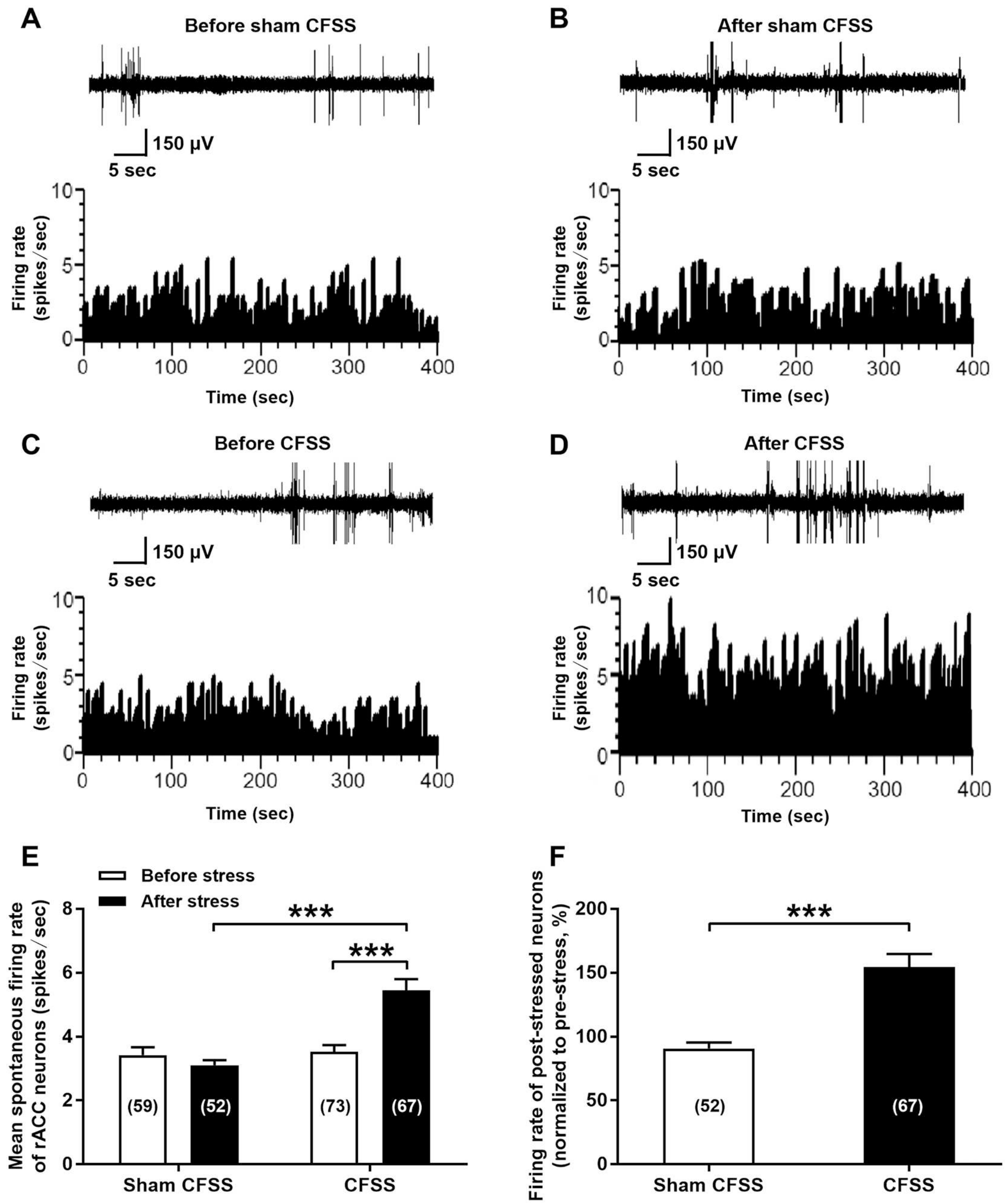

Fig. 2. Effects of chronic forced swim stress (CFSS) on the baseline activity of rACC neurons in rats. (A–D): Representative baseline firing activity of rACC neurons in rats exposed to sham CFSS (A, B) or CFSS (C, D). Histogram display the firing rate (spikes per second) of rACC neurons during a 400-s time-window sampling. Bin width = 1 s. Insets show the original traces of the spontaneous firing activity recorded from rACC neurons. Scale bar: 150 μV, 5 s. (E): Averaged spontaneous firing rate of rACC neurons in different groups. Note that the mean spontaneous firing rate of rACC neurons is significantly increased in rats exposed to CFSS. ***P < 0.001, two-way ANOVA followed by Bonferroni post-hoc test, n = 52–73 neurons per group. (F): Normalized firing rate of post-stressed rACC neurons relative to the mean baseline activity of pre-stressed rACC neurons in CFSS- and sham CFSS-treated rats, respectively. ***P < 0.001, two-tailed unpaired t-test, n = 52–67 neurons per group.

two-way ANOVA, Fig. 3E). Additionally, after exposure of stress, both the LIS-evoked firing rate (in spikes/s, 10.07 ± 0.46 CFSS vs. 4.51 ± 0.31 sham CFSS, $F_{1,161}$ = 61.64, P < 0.0001) and the HNS-evoked firing rate (in spikes/s, 22.86 ± 0.51 CFSS vs. 7.78 ± 0.44 sham CFSS, $F_{1,166}$ = 239.6, P < 0.0001) of rACC neurons were significantly increased in CFSS-treated rats compared with the sham CFSS-treated rats (two-way ANOVA, Fig. 3B and E). Likewise, after exposure of stress, the normalized firing rate of rACC neurons relative to the mean laser-evoked activity of pre-stress was significantly increased in CFSS-treated rats compared with the sham CFSS-treated rats, both by LIS (236.6 ± 10.8% of pre-stress in CFSS-treated rats vs. 90.1 ± 6.3% of pre-sham stress in sham CFSS-treated rats, t_{77} = 10.41, P < 0.0001) and by HNS (266.5 ± 6.0% of pre-stress in CFSS-treated rats vs. 77.5 ± 6.5% of pre-sham stress in sham CFSS-treated rats, t_{80} = 21.21, P < 0.0001) to rats (unpaired two-tailed t-test, Fig. 3C and F). These findings indicated that exposure of CFSS to rats could also enhance the laser-evoked activity of rACC neurons either by LIS or HNS, thereby validating our understanding that chronic stress could induce a sensitization of rACC neurons in rats.

3.4. Chronic forced swim stress enhances the baseline field potential power of rACC local field potential in rats

Furthermore, we tested whether chronic stress would change the

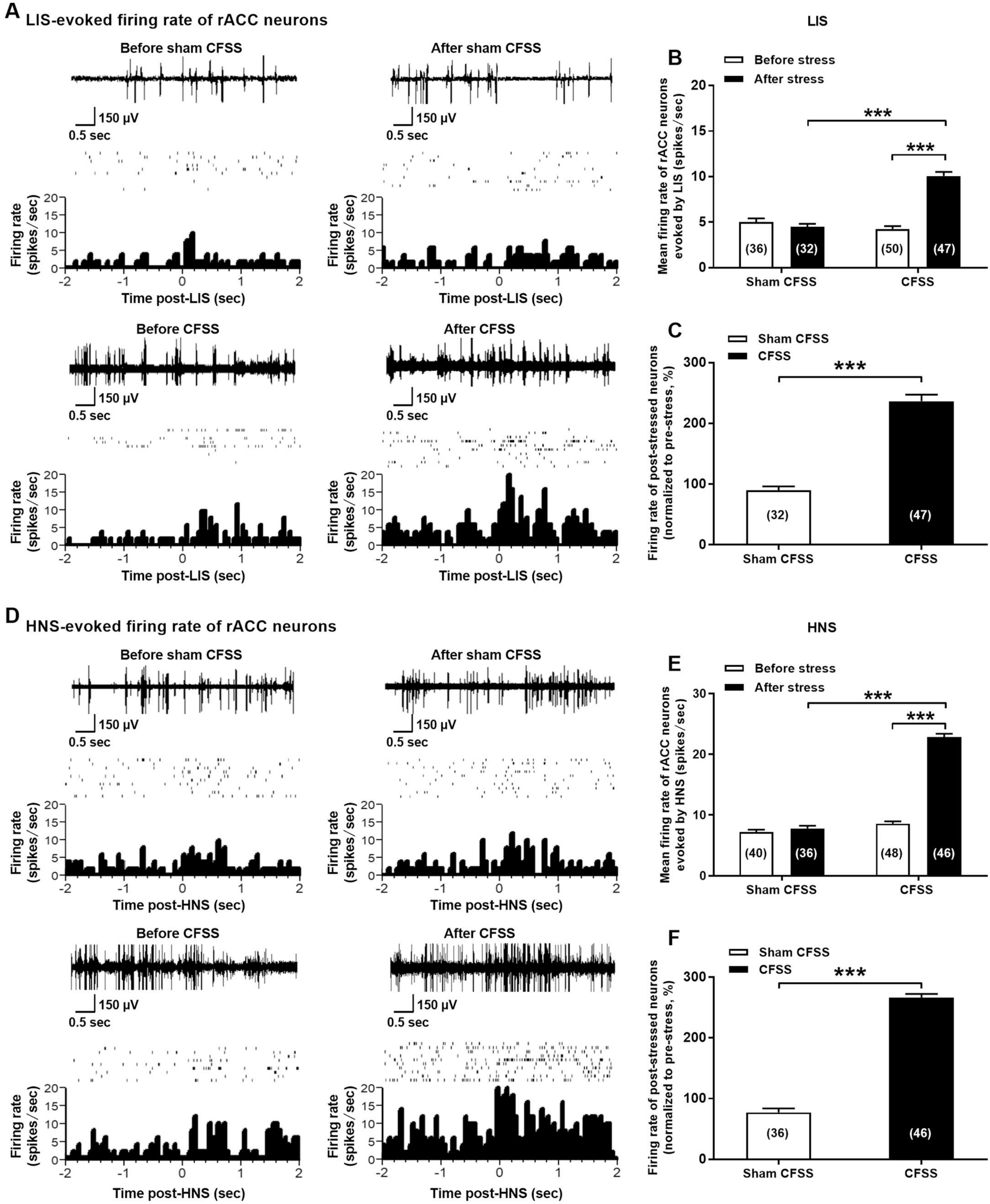

(caption on next page)

Fig. 3. Effects of chronic forced swim stress (CFSS) on innoxious- and noxious-laser stimuli-evoked activity of rACC neurons in rats. (A–C): Low intensity innoxious stimuli (LIS)-evoked firing activity of rACC neurons in CFSS- and sham CFSS-treated rats. (A): Representative LIS-evoked firing activity of rACC neurons in rats exposed to CFSS or sham CFSS. Histogram display the firing rate (spikes per second) of rACC neurons during a time-window from the 2 s before laser stimuli to the 2 s after laser stimuli. Bin width = 50 milliseconds. Insets show the original traces of the laser-evoked firing of rACC neurons (up) and the scatter diagram of spikes distribution (bottom). Scale bar: 150 μV, 0.5 s. (B): Averaged firing rate of LIS-evoked rACC neurons activity in different groups. Note that the mean laser-evoked firing rate of rACC neurons is significantly increased in rats exposed to CFSS. ***$P < 0.001$, two-way ANOVA followed by Bonferroni post-hoc test, $n = 32–50$ neurons per group. (C): Normalized firing rate of rACC neurons after stress relative to the mean laser-evoked activity of rACC neurons before stress in CFSS- and sham CFSS-treated rats, respectively. ***$P < 0.001$, two-tailed unpaired t-test, $n = 32–47$ neurons per group. (D–F): High intensity noxious stimuli (HNS)-evoked firing activity of rACC neurons in CFSS- and sham CFSS-treated rats. (D): Representative HNS-evoked firing activity of rACC neurons in rats exposed to CFSS or sham CFSS. Histogram display the firing rate (spikes per second) of rACC neurons during a time-window from the 2 s before laser stimuli to the 2 s after laser stimuli. Bin width = 50 milliseconds. Insets show the original traces of the laser-evoked firing of rACC neurons (up) and the scatter diagram of spikes distribution (bottom). Scale bar: 150 μV, 0.5 s. (E): Averaged firing rate of HNS-evoked rACC neurons activity in different groups. Note that the mean laser-evoked firing rate of rACC neurons is significantly increased in rats exposed to CFSS. ***$P < 0.001$, two-way ANOVA followed by Bonferroni post-hoc test, $n = 36–48$ neurons per group. (F): Normalized firing rate of rACC neurons after stress relative to the mean laser-evoked activity of rACC neurons before stress in CFSS- and sham CFSS-treated rats, respectively. ***$P < 0.001$, two-tailed unpaired t-test, $n = 36–46$ neurons per group.

baseline field potential power (FPP) of rACC local field potential (LFP) in rats. In this study, LFP signals were filtered into five frequency bands: theta (4–8 Hz), alpha (9–12 Hz), beta (13–30 Hz), low gamma (31–70 Hz), and high gamma (71–100 Hz), in which the theta, alpha and beta bands belong to the low frequency band (4–30 Hz), while the low gamma and high gamma bands belong to the high frequency band (31–100 Hz). As analyzed for the broadband (4–100 Hz) frequency range LFP, we found a significant increase in filed potential power (FPP) of rACC LFP after CFSS, in which the main alteration was displayed in low frequency range LFP (Fig. 4). Here, Fig. 4A shows an example of raw LFP waveform and the grand averaged time-frequency distribution of rACC FPP in CFSS- and sham CFSS-treated rats, before and after stress; Fig. 4B and C show a representative FPP of rACC LFP and the averaged FPP in CFSS- and sham CFSS-treated rats, before and after stress, in which we found an increased FPP in the low frequency band (4–30 Hz) LFP in rats after CFSS compared with the other three control groups (before CFSS, before and after sham CFSS). As normalized to the pre-stress, we found that the normalized FPP of post-stress was also augmented in a broadband (4–100 Hz) frequency range LFP in CFSS-treated rats compared with sham CFSS-treated rats (Fig. 4D). The FPP histogram also revealed that as compared with before CFSS or after sham CFSS, the FPP of rACC LFP (in $\mu V^2/Hz$) was significantly increased both in low frequency band (4–30 Hz) (0.014 ± 0.003 post-CFSS vs. $0.6 \times 10^{-4} \pm 0.3 \times 10^{-5}$ pre-CFSS vs. $0.8 \times 10^{-4} \pm 0.2 \times 10^{-4}$ post-sham CFSS, $P < 0.0001$) and in broadband (4–100 Hz) frequency range (0.005 ± 0.001 post-CFSS vs. $0.2 \times 10^{-4} \pm 0.1 \times 10^{-5}$ pre-CFSS vs. $0.3 \times 10^{-4} \pm 0.47 \times 10^{-5}$ post-sham CFSS, $P = 0.0172$ vs. pre-CFSS; $P = 0.0399$ vs. post-sham CFSS) after exposure of CFSS to rats ($F_{6,48} = 7.205$, two-way ANOVA, Fig. 4E).

Similarly, as analyzed for the low frequency band (4–30 Hz) FPP of rACC LFP, we also found a prominent increase in rACC FPP after CFSS (Fig. 4F to J), in which the Fig. 4F shows a grand averaged time-frequency distribution of rACC FPP in the low frequency band (4–30 Hz) LFP in CFSS- and sham CFSS-treated rats, before and after stress; Fig. 4G and H show a representative FPP of rACC LFP and the averaged FPP in the four groups, while Fig. 4I shows the normalized FPP of post-stress relative to pre-stress in CFSS and sham CFSS groups. The FPP histogram revealed that compared with pre-CFSS or post-sham CFSS, the FPP of rACC LFP (in $\mu V^2/Hz$) was significantly increased in theta (0.044 ± 0.011 post-CFSS vs. $0.2 \times 10^{-3} \pm 0.1 \times 10^{-4}$ pre-CFSS vs. $0.3 \times 10^{-3} \pm 0.5 \times 10^{-4}$ post-sham CFSS, $P < 0.0001$) and alpha (0.018 ± 0.004 post-CFSS vs. $0.1 \times 10^{-3} \pm 0.4 \times 10^{-5}$ pre-CFSS vs. $0.1 \times 10^{-3} \pm 0.2 \times 10^{-4}$ post-sham CFSS, $P = 0.0107$ vs. pre-CFSS; $P = 0.0272$ vs. post-sham CFSS) frequency bands, but not in beta frequency band (0.006 ± 0.002 post-CFSS vs. $0.25 \times 10^{-4} \pm 0.21 \times 10^{-5}$ pre-CFSS vs. $0.29 \times 10^{-4} \pm 0.1 \times 10^{-4}$ post-sham CFSS, $P = 0.6386$ vs. pre-CFSS; $P = 0.7152$ vs. post-sham CFSS) after exposure of CFSS to rats ($F_{6,48} = 5.906$, two-way ANOVA, Fig. 4J).

In addition, as analyzed for the high frequency band (31–100 Hz) FPP of rACC LFP, we found that the rACC FPP was also increased in the CFSS-treated rats after stress (Fig. 4K to O). Fig. 4K shows a grand averaged time-frequency distribution of rACC FPP in the high frequency band (31–100 Hz) LFP in CFSS- and sham CFSS-treated rats, before and after stress. Fig. 4L and M show a representative FPP of rACC LFP and the averaged FPP in the four groups, while Fig. 4N shows the normalized FPP of post-stress relative to pre-stress in CFSS and sham CFSS groups. The FPP histogram disclosed that compared with pre-CFSS or post-sham CFSS, the FPP of rACC LFP (in $\mu V^2/Hz$) was significantly increased in low gamma ($0.001 \pm 0.3 \times 10^{-3}$ post-CFSS vs. $0.9 \times 10^{-5} \pm 0.1 \times 10^{-5}$ pre-CFSS vs. $0.9 \times 10^{-5} \pm 0.95 \times 10^{-6}$ post-sham CFSS, $P < 0.0001$) but not in high gamma frequency band ($0.4 \times 10^{-3} \pm 0.1 \times 10^{-3}$ post-CFSS vs. $0.4 \times 10^{-5} \pm 0.46 \times 10^{-6}$ pre-CFSS vs. $0.5 \times 10^{-5} \pm 0.43 \times 10^{-6}$ post-sham CFSS, $P = 0.0947$ vs. pre-CFSS; $P = 0.1587$ vs. post-sham CFSS) after CFSS ($F_{3,32} = 7.056$, two-way ANOVA, Fig. 4O).

These data suggested that exposure of CFSS to rats could increase the baseline FPP of rACC LFP, especially in low frequency theta and alpha bands as well as in high frequency low gamma band ranges.

3.5. Chronic forced swim stress enhances the FPP of rACC LFP induced by low intensity innoxious stimuli (LIS) and high intensity noxious stimuli (HNS) to rats

Apart from the baseline FPP of rACC LFP, we found that exposure of CFSS to rats could also enhance the FPP of rACC LFP induced by LIS and HNS to rats. Fig. 5 depicts the LIS-induced FPP of rACC LFP in CFSS- and sham CFSS-treated rats, in which the Fig. 5A shows an example of raw LFP waveform and the grand averaged time-frequency distribution of rACC FPP in CFSS- and sham CFSS-treated rats, before and after stress; Fig. 5B and C show a representative FPP of rACC LFP and the averaged FPP in CFSS- and sham CFSS-treated rats, before and after stress, in which we found an increased FPP in the low frequency band (4–30 Hz) LFP in rats after CFSS compared with the other three control groups (before CFSS, before and after sham CFSS). Likewise, the normalized FPP of post-stress relative to pre-stress was mainly increased in the low frequency range LFP in CFSS-treated rats compared with sham CFSS-treated rats (Fig. 5D). The FPP histogram also revealed that the FPP of rACC LFP (in $\mu V^2/Hz$) was significantly increased in the low frequency range ($0.6 \times 10^{-3} \pm 0.3 \times 10^{-3}$ post-CFSS vs. $0.1 \times 10^{-3} \pm 0.4 \times 10^{-4}$ pre-CFSS vs. $0.1 \times 10^{-3} \pm 0.4 \times 10^{-4}$ post-sham CFSS, $F_{6,36} = 0.738$, $P = 0.0153$ vs. pre-CFSS; $P = 0.0318$ vs. post-sham CFSS) after CFSS as compared with pre-CFSS or post-sham CFSS (two-way ANOVA, Fig. 5E).

As further analyzed for the low frequency band (4–30 Hz) FPP of rACC LFP, we also found a remarkable increase in rACC FPP after CFSS (Fig. 5F to I), in which the Fig. 5F and G show a representative FPP of rACC LFP and the averaged FPP in the four groups, while Fig. 5H shows the normalized FPP of post-stress relative to pre-stress in CFSS and sham CFSS groups. The FPP histogram disclosed that compared with

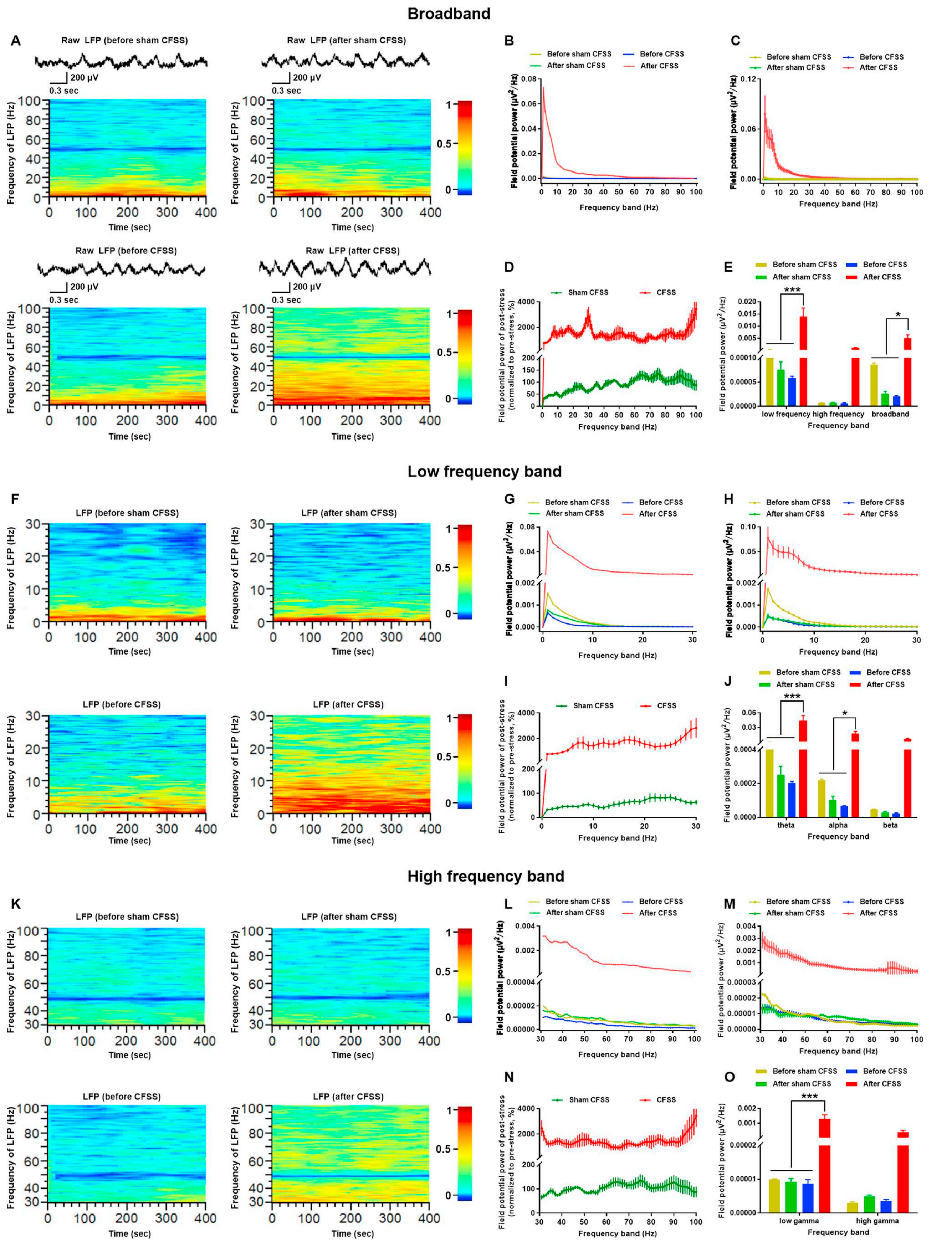

(caption on next page)

Fig. 4. Effects of chronic forced swim stress (CFSS) on baseline field potential power (FPP) activity of rACC local field potential (LFP) in rats. (A–E): Analysis of rACC FPP in the broadband (4–100 Hz) frequency range LFP. (A): Representative examples of raw LFP waveform and the grand averaged time-frequency distribution of rACC FPP in CFSS- and sham CFSS-treated rats, before and after stress. Scale bar: 200 μV, 0.3 s. Warm and cool colors indicate the increase and decrease in FPP activity of rACC LFP, respectively. (B and C): Show a representative FPP of rACC LFP and the averaged FPP in CFSS- and sham CFSS-treated rats, before and after stress. (D): Normalized FPP of post-stress relative to pre-stress in CFSS- and sham CFSS-treated rats. (E): Histogram of rACC FPP in low frequency (4–30 Hz), high frequency (31–100 Hz), and the broadband (4–100 Hz) frequency ranges LFP. *$P < 0.05$, ***$P < 0.001$, two-way ANOVA followed by Tukey's multiple comparisons test, $n = 4$–6 rats per group. (F–J): Analysis of low frequency band (4–30 Hz) FPP of rACC LFP. (F): Grand averaged time-frequency distribution of rACC FPP in low frequency band LFP in CFSS- and sham CFSS-treated rats, before and after stress. Warm and cool colors indicate the increase and decrease in FPP activity of rACC LFP, respectively. (G and H): Show a representative FPP of rACC LFP and the averaged FPP in CFSS- and sham CFSS-treated rats, before and after stress. (I): Normalized FPP of post-stress relative to pre-stress in CFSS- and sham CFSS-treated rats. (J): Histogram of rACC FPP in theta (4–8 Hz), alpha (9–12 Hz) and beta (13–30 Hz) frequency ranges LFP. *$P < 0.05$, ***$P < 0.001$, two-way ANOVA followed by Tukey's multiple comparisons test, $n = 4$–6 rats per group. (K–O): Analysis of high frequency band (31–100 Hz) FPP of rACC LFP. (K): Grand averaged time-frequency distribution of rACC FPP in high frequency band LFP in CFSS- and sham CFSS-treated rats, before and after stress. Warm and cool colors indicate the increase and decrease in FPP activity of rACC LFP, respectively. (L and M): Show a representative FPP of rACC LFP and the averaged FPP in CFSS- and sham CFSS-treated rats, before and after stress. (N): Normalized FPP of post-stress relative to pre-stress in CFSS- and sham CFSS-treated rats. (O): Histogram of rACC FPP in low gamma (31–70 Hz) and high gamma (71–100 Hz) frequency ranges LFP. ***$P < 0.001$, two-way ANOVA followed by Tukey's multiple comparisons test, $n = 4$–6 rats per group.

pre-CFSS or post-sham CFSS, the FPP of rACC LFP (in μV^2/Hz) was significantly increased in theta frequency band ($0.002 \pm 0.9 \times 10^{-3}$ post-CFSS vs. $0.5 \times 10^{-3} \pm 0.2 \times 10^{-3}$ pre-CFSS vs. $0.6 \times 10^{-3} \pm 0.2 \times 10^{-3}$ post-sham CFSS, $F_{6,36} = 0.6379$, $P = 0.0296$ vs. pre-CFSS; $P = 0.0492$ vs. post-sham CFSS) after CFSS (two-way ANOVA, Fig. 5I).

However, as analyzed for the high frequency band (31–100 Hz) FPP of rACC LFP, no significant difference was observed on the rACC FPP between CFSS- and sham CFSS-treated rats (Fig. 5J to M). Fig. 5J and K show a representative FPP of rACC LFP and the averaged FPP in the four groups, while Fig. 5L shows the normalized FPP of post-stress relative to pre-stress in CFSS and sham CFSS groups. As compared with pre-CFSS or post-sham CFSS, the FPP of rACC LFP (in μV^2/Hz) had no significant alteration either in low gamma ($P = 0.7676$ vs. pre-CFSS; $P = 0.1122$ vs. post-sham CFSS) or in high gamma frequency band ($P = 0.9955$ vs. pre-CFSS; $P = 0.9746$ vs. post-sham CFSS) after exposure of CFSS to rats ($F_{3,24} = 1.049$, two-way ANOVA, Fig. 5M).

With respect to the HNS-induced FPP of rACC LFP, Fig. 6A shows an example of raw LFP waveform and the grand averaged time-frequency distribution of rACC FPP in CFSS- and sham CFSS-treated rats, before and after stress; Fig. 6B and C show a representative of rACC LFP and the averaged FPP in CFSS- and sham CFSS-treated rats, before and after stress, in which we also observed a prominent increase mainly in the low frequency (4–30 Hz) LFP in rats after CFSS compared with the other three control groups (before CFSS, before and after sham CFSS). However, the normalized FPP of post-stress relative to pre-stress was increased in a broadband (4–100 Hz) frequency range LFP in CFSS-treated rats compared with sham CFSS-treated rats (Fig. 6D). The FPP histogram showed that compared with pre-CFSS or post-sham CFSS, the FPP of rACC LFP (in μV^2/Hz) was significantly increased both in low frequency band (4–30 Hz) (0.006 ± 0.001 post-CFSS vs. $0.1 \times 10^{-3} \pm 0.\ 6 \times 10^{-4}$ pre-CFSS vs. $0.2 \times 10^{-3} \pm 0.\ 1 \times 10^{-3}$ post-sham CFSS, $P < 0.0001$) and in broadband (4–100 Hz) ($0.002 \pm 0.4 \times 10^{-3}$ post-CFSS vs. $0.1 \times 10^{-3} \pm 0.9 \times 10^{-4}$ pre-CFSS vs. $0.1 \times 10^{-3} \pm 0.1 \times 10^{-3}$ post-sham CFSS, $P = 0.0105$ vs. pre-CFSS; $P = 0.0116$ vs. post-sham CFSS) frequency ranges after CFSS ($F_{6,36} = 8.427$, two-way ANOVA, Fig. 6E).

As analyzed for the low frequency band (4–30 Hz) FPP of rACC LFP, we also found an obvious increase in rACC FPP after CFSS (Fig. 6F to I), in which the Fig. 6F and G show a representative FPP of rACC LFP and averaged FPP in the four groups, while Fig. 6H shows the normalized FPP of post-stress relative to pre-stress in CFSS and sham CFSS groups. The FPP histogram uncovered that compared with pre-CFSS or post-sham CFSS, the FPP of rACC LFP (in μV^2/Hz) was significantly increased in theta frequency band (0.03 ± 0.01 post-CFSS vs. $0.6 \times 10^{-3} \pm 0.3 \times 10^{-3}$ pre-CFSS vs. $0.001 \pm 0.5 \times 10^{-3}$ post-sham CFSS, $F_{6,36} = 8.498$, $P < 0.0001$) after exposure of CFSS to rats (two-way ANOVA, Fig. 6I).

Also, as analyzed for the high frequency band (31–100 Hz) FPP of rACC LFP, we found that the rACC FPP was increased in CFSS-treated rats after stress (Fig. 6J to M), in which the Fig. 6J and K show a representative FPP of rACC LFP and the averaged FPP in the four groups, while Fig. 6L shows the normalized FPP of post-stress relative to pre-stress in CFSS and sham CFSS groups. The FPP histogram showed that compared with pre-CFSS or post-sham CFSS, the FPP of rACC LFP (in μV^2/Hz) was significantly increased in low gamma ($0.001 \pm 0.4 \times 10^{-3}$ post-CFSS vs. $0.2 \times 10^{-3} \pm 0.2 \times 10^{-3}$ pre-CFSS vs. $0.2 \times 10^{-3} \pm 0.2 \times 10^{-3}$ post-sham CFSS, $P = 0.0026$ vs. pre-CFSS; $P = 0.0027$ vs. post-sham CFSS) but not in high gamma ($P = 0.5345$ vs. pre-CFSS; $P = 0.5360$ vs. post-sham CFSS) frequency band after CFSS ($F_{3,24} = 2.046$, two-way ANOVA, Fig. 6M).

Altogether, these results indicated that exposure of CFSS to rats could also increase the FPP of rACC LFP induced by LIS and HNS to rats, especially in low frequency theta band as well as in high frequency low gamma band ranges.

3.6. Chronic forced swim stress promotes the synchronization between rACC and BLA, and increases the neural information flow from rACC to BLA

To further investigate the spatial and temporal correlation and the functional connectivity between rACC and BLA regions, we employed a method using the cross-correlation of the instantaneous amplitudes of band-pass filtered LFPs (Adhikari et al., 2010), which were evoked by LIS and HNS to rats, to calculate coherence values between rACC and BLA regions. The coherence values can be positive (i.e. activities in the two regions tends to go up and down together) or negative (i.e. activities in one region correlates with less activity in another region, and vice-versa) (Harris and Gordon, 2015), and the larger the absolute value, the higher the correlation. In addition, the occurrence of negative lags at the coherence peak indicates that one brain region leads another brain region, and vice-versa, while the close to-zero lag means the simultaneous activity between the two regions. Moreover, in order to further explore the directionality of the neural information flow between the brain regions during the encoding of nociceptive information process, we introduced the partial directed coherence (PDC) algorithm (Li et al., 2018). The closer the PDC value, a vector length, is to 1, the greater the influence of one brain region on another region, and vice versa. While the PDC value is close to 0, the influence between the two brain regions is symmetric.

Fig. 7A to F depict the coherence and PDC analysis for LIS-induced LFP between rACC and BLA regions in rats exposed to CFSS or sham CFSS, in which the Fig. 7A shows an example of representative traces of LIS-evoked LFP in rACC and BLA, respectively, to indicate the high synchronization between the two brain regions in rats after exposure of CFSS. The occurrence of the close to-zero lag for the rACC–BLA cross-correlation peak provided a substantial validation for this synchronization between the two brain regions after exposure of CFSS. Furthermore, to examine the in-depth characteristics of the synergic activity

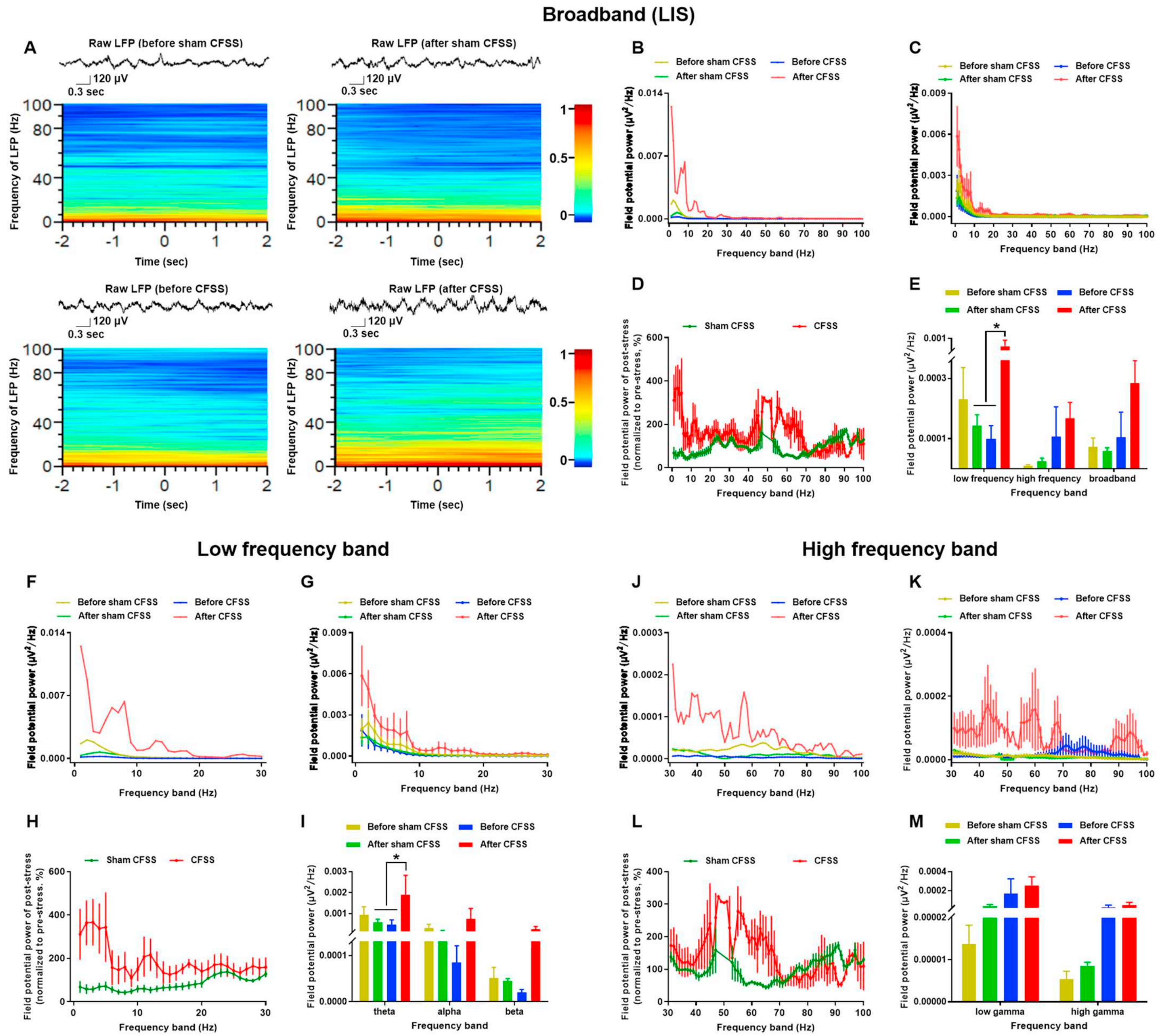

Fig. 5. Effects of chronic forced swim stress (CFSS) on the field potential power (FPP) activity of rACC local field potential (LFP) induced by low intensity innoxious stimuli (LIS) to rats. (A–E): Analysis of rACC FPP in the broadband (4–100 Hz) frequency range LFP. (A): Representative examples of raw LFP waveform and the grand averaged time-frequency distribution of rACC FPP in CFSS- and sham CFSS-treated rats, before and after stress. Scale bar: 120 μV, 0.3 s. Warm and cool colors indicate the increase and decrease in FPP activity of rACC LFP, respectively. (B and C): Show a representative FPP of rACC LFP and the averaged FPP in CFSS- and sham CFSS-treated rats, before and after stress. (D): Normalized FPP of post-stress relative to pre-stress in CFSS- and sham CFSS-treated rats. (E): Histogram of rACC FPP in low frequency (4–30 Hz), high frequency (31–100 Hz), and the broadband (4–100 Hz) frequency ranges LFP. *$P < 0.05$, two-way ANOVA followed by Tukey's multiple comparisons test, $n = 4$ rats per group. (F–I): Analysis of low frequency band (4–30 Hz) FPP of rACC LFP. (F and G): Show a representative FPP of rACC LFP and the averaged FPP in CFSS- and sham CFSS-treated rats, before and after stress. (H): Normalized FPP of post-stress relative to pre-stress in CFSS- and sham CFSS-treated rats. (I): Histogram of rACC FPP in theta (4–8 Hz), alpha (9–12 Hz) and beta (13–30 Hz) frequency ranges LFP. *$P < 0.05$, two-way ANOVA followed by Tukey's multiple comparisons test, $n = 4$ rats per group. (J–M): Analysis of high frequency band (31–100 Hz) FPP of rACC LFP. (J and K): Show a representative FPP of rACC LFP and the averaged FPP in CFSS- and sham CFSS-treated rats, before and after stress. (L): Normalized FPP of post-stress relative to pre-stress in CFSS- and sham CFSS-treated rats. (M): Histogram of rACC FPP in low gamma (31–70 Hz) and high gamma (71–100 Hz) frequency ranges LFP. $P > 0.05$, compared between post-CFSS and pre-CFSS or between post-CFSS and post-sham CFSS, two-way ANOVA followed by Tukey's multiple comparisons test, $n = 4$ rats per group.

between the rACC and BLA regions, we also analyzed the cross-correlation for LIS-evoked LFP amplitudes between low (4–30 Hz) and low (low-low), high (31–100 Hz) and high (high-high), as well as low and high (low-high) frequency bands in rACC and BLA regions after exposure of CFSS to rats. The results showed that the coherence coefficient between low and low (0.87 ± 0.03 post-CFSS vs. 0.45 ± 0.04 pre-CFSS vs. 0.53 ± 0.01 post-sham CFSS, $P < 0.0001$ vs. pre-CFSS or post-sham CFSS), high and high (0.94 ± 0.02 post-CFSS vs. 0.47 ± 0.04 pre-CFSS vs. 0.41 ± 0.05 post-sham CFSS, $P < 0.0001$ vs. pre-CFSS or post-sham CFSS) and, low and high (0.95 ± 0.02 post-CFSS vs. 0.36 ± 0.06 pre-CFSS vs. 0.50 ± 0.02 post-sham CFSS, $P < 0.0001$ vs. pre-CFSS or post-sham CFSS) frequency bands, were significantly increased after stress in the CFSS-treated rats as compared with the control groups ($F_{6,59} = 2.847$, two-way ANOVA, Fig. 7C). Likewise, the coherence coefficient between theta and theta (0.93 ± 0.03 post-CFSS vs. 0.47 ± 0.04 pre-CFSS vs. 0.43 ± 0.06

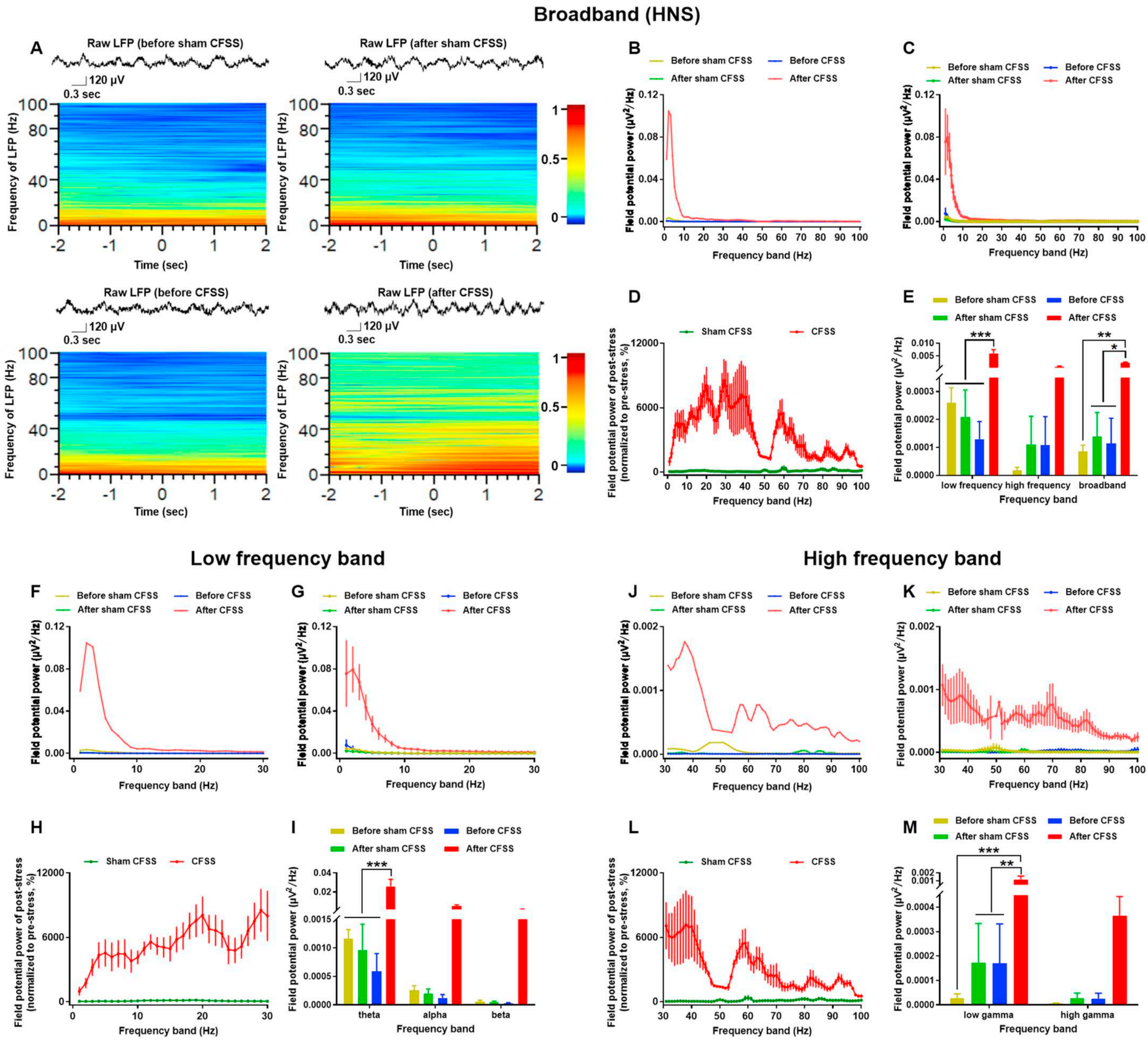

Fig. 6. Effects of chronic forced swim stress (CFSS) on the field potential power (FPP) activity of rACC local field potential (LFP) induced by high intensity noxious stimuli (HNS) to rats. (A–E): Analysis of rACC FPP in the broadband (4–100 Hz) frequency range LFP. (A): Representative examples of raw LFP waveform and the grand averaged time-frequency distribution of rACC FPP in CFSS- and sham CFSS-treated rats, before and after stress. Scale bar: 120 μV, 0.3 s. Warm and cool colors indicate the increase and decrease in FPP activity of rACC LFP, respectively. (B and C): Show a representative FPP of rACC LFP and the averaged FPP in CFSS- and sham CFSS-treated rats, before and after stress. (D): Normalized FPP of post-stress relative to pre-stress in CFSS- and sham CFSS-treated rats. (E): Histogram of rACC FPP in low frequency (4–30 Hz), high frequency (31–100 Hz), and the broadband (4–100 Hz) frequency ranges LFP. *P < 0.05, ***P < 0.001, two-way ANOVA followed by Tukey's multiple comparisons test, $n = 4$ rats per group. (F–I): Analysis of low frequency band (4–30 Hz) FPP of rACC LFP. (F and G): Show a representative FPP of rACC LFP and the averaged FPP in CFSS- and sham CFSS-treated rats, before and after stress. (H): Normalized FPP of post-stress relative to pre-stress in CFSS- and sham CFSS-treated rats. (I): Histogram of rACC FPP in theta (4–8 Hz), alpha (9–12 Hz) and beta (13–30 Hz) frequency ranges LFP. ***P < 0.001, two-way ANOVA followed by Tukey's multiple comparisons test, $n = 4$ rats per group. (J–M): Analysis of high frequency band (31–100 Hz) FPP of rACC LFP. (J and K): Show a representative FPP of rACC LFP and the averaged FPP in CFSS- and sham CFSS-treated rats, before and after stress. (L): Normalized FPP of post-stress relative to pre-stress in CFSS- and sham CFSS-treated rats. (M): Histogram of rACC FPP in low gamma (31–70 Hz) and high gamma (71–100 Hz) frequency ranges LFP. **P < 0.01, two-way ANOVA followed by Tukey's multiple comparisons test, $n = 4$ rats per group.

post-sham CFSS, P < 0.0001 vs. pre-CFSS or post-sham CFSS), low gamma and low gamma (0.93 ± 0.02 post-CFSS vs. 0.45 ± 0.05 pre-CFSS vs. 0.50 ± 0.02 post-sham CFSS, P < 0.0001 vs. pre-CFSS or post-sham CFSS) and, theta and low gamma (0.91 ± 0.04 post-CFSS vs. 0.53 ± 0.05 pre-CFSS vs. 0.55 ± 0.03 post-sham CFSS, P < 0 .0001 vs. pre-CFSS or post-sham CFSS) frequency bands, were also significantly increased after stress in CFSS-treated rats ($F_{6,60} = 1.271$, two-way ANOVA, Fig. 7D). However, between CFSS- and sham CFSS-treated rats, no significant difference was observed either on the absolute PDC values (P > 0.9999, $F_{12,80} = 0.264$, two-way ANOVA, Fig. 7E), or on the normalized PDC values of post-stress LFP relative to pre-stress LFP (P = 0.9997, $F_{4,30} = 0.317$, two-way ANOVA, Fig. 7F) at the rACC–BLA pathway.

Similarly, Fig. 7G to L describe the coherence and PDC analysis for

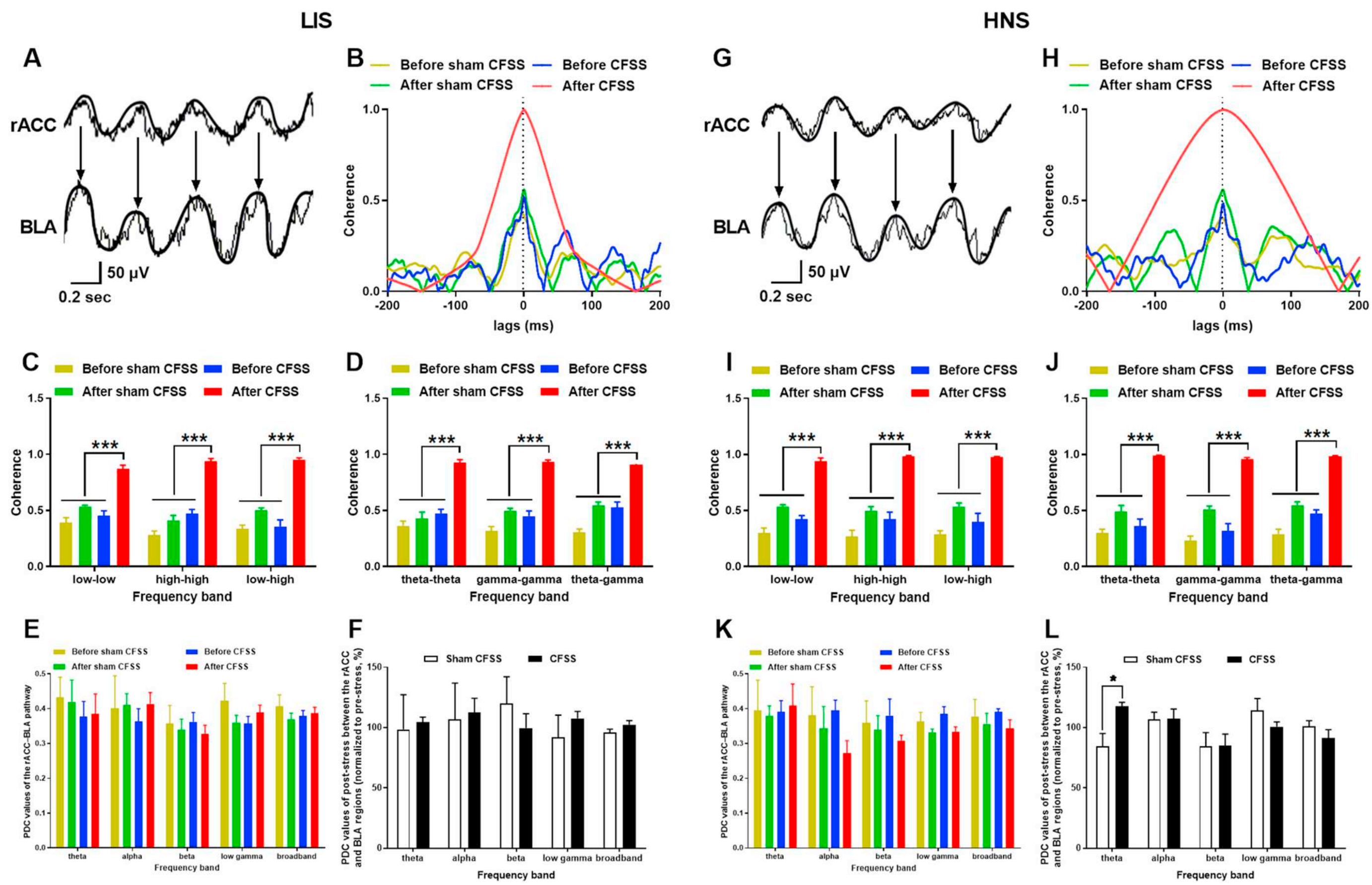

Fig. 7. Effects of chronic forced swim stress (CFSS) on the functional connectivity and the directionality of neural information flow between rACC and BLA regions. Coherence and PDC analysis for LIS-induced LFP (A–F) and HNS-induced LFP (G–L) between rACC and BLA regions are shown. (A and G): Show an example of representative traces of LIS-evoked LFP (A) and HNS-evoked LFP (G) in rACC and BLA, respectively, to indicate the high synchronization between the two brain regions in rats after exposure of CFSS. Scale bar: 50 μV, 0.2 s. (B and H): Representative traces show the lags of rACC-BLA LFP coherence respectively induced by LIS (B) and HNS (H) in CFSS- and sham CFSS-treated rats. Note that the occurrence of the close to-zero lag for the rACC–BLA cross-correlation peak provided a substantial validation for this synchronization between the two brain regions after exposure of CFSS. (C and I): The cross-correlation analysis for LIS-evoked LFP amplitudes (C) and HNS-evoked LFP amplitudes (I) between low (4–30 Hz) and low (low-low), high (31–100 Hz) and high (high-high), as well as low and high (low-high) frequency bands in rACC and BLA regions after exposure of CFSS to rats. ***P < 0.001, two-way ANOVA followed by Tukey's multiple comparisons test, n = 4–6 rats per group. (D and J): The cross-correlation analysis for LIS-evoked LFP amplitudes (C) and HNS-evoked LFP amplitudes (I) between theta and theta, low gamma and low gamma, as well as theta and low gamma frequency bands in rACC and BLA regions after exposure of CFSS to rats. ***P < 0.001, two-way ANOVA followed by Tukey's multiple comparisons test, n = 4–6 rats per group. (E and K): Partial directed coherence (PDC) analysis for LIS-evoked LFP (E) and HNS-evoked LFP (K) between rACC and BLA regions in CFSS- and sham CFSS-treated rats. P > 0.05, two-way ANOVA followed by Tukey's multiple comparisons test, n = 4–6 rats per group. (F and L): Normalized PDC values of post-stress LFP relative to pre-stress LFP, evoked by LIS (F) and HNS (L), in CFSS- and sham CFSS-treated rats. *P < 0.05, two-way ANOVA followed by Tukey's multiple comparisons test, n = 4–6 rats per group.

HNS-induced LFP between rACC and BLA regions in rats exposed to CFSS or sham CFSS, in which Fig. 7G shows an example of representative traces of HNS-evoked LFP in rACC and BLA, respectively, to indicate the high synchronization between the two brain regions in rats after exposure of CFSS. The occurrence of the close to-zero lag for the rACC–BLA correlation peak also provided a solid validation for this synchronization between the two brain regions after exposure of CFSS. The coherence coefficient for HNS-evoked LFP amplitudes between low and low (0.94 ± 0.03 post-CFSS vs. 0.42 ± 0.03 pre-CFSS vs. 0.53 ± 0.02 post-sham CFSS, P < 0.0001 vs. pre-CFSS or post-sham CFSS), high and high (0.99 ± 0.03 post-CFSS vs. 0.42 ± 0.06 pre-CFSS vs. 0.50 ± 0.04 post-sham CFSS, P < 0.0001 vs. pre-CFSS or post-sham CFSS) and, low and high (0.98 ± 0.01 post-CFSS vs. 0.40 ± 0.08 pre-CFSS vs. 0.54 ± 0.03 post-sham CFSS, P < 0.0001 vs. pre-CFSS or post-sham CFSS) frequency bands, were also significantly increased after stress in CFSS-treated rats ($F_{6,60}$ = 0.280, two-way ANOVA, Fig. 7I). Accordantly, the coherence coefficient between theta and theta (0.99 ± 0.01 post-CFSS vs. 0.36 ± 0.06 pre-CFSS vs. 0.49 ± 0.06 post-sham CFSS, P < 0.0001 vs. pre-CFSS or post-sham CFSS), low gamma and low gamma (0.96 ± 0.02 post-CFSS vs. 0.32 ± 0.07 pre-CFSS vs. 0.51 ± 0.03 post-sham CFSS, P < 0.0001 vs. pre-CFSS or post-sham CFSS) and, theta and low gamma (0.99 ± 0.01 post-CFSS vs. 0.47 ± 0.03 pre-CFSS vs. 0.55 ± 0.03 post-sham CFSS, P < 0.0001 vs. pre-CFSS or post-sham CFSS) frequency bands, were also significantly increased after stress in CFSS-treated rats ($F_{6,60}$ = 0.862, two-way ANOVA, Fig. 7J). Although no significant difference was observed on the absolute PDC values (P > 0.9999, $F_{12,80}$ = 0.374, two-way ANOVA, Fig. 7K), the normalized PDC values of post-stress LFP relative to pre-stress LFP at the rACC–BLA pathway was significantly increased (117.6 ± 8.1% CFSS vs. 84.4 ± 18.5% sham CFSS, $F_{4,37}$ = 2.403, P = 0.0437) in theta frequency band in rats exposed to CFSS (two-way ANOVA, Fig. 7L).

Taken together, the aforementioned data suggested that exposure of chronic FS stress to rats not only promoted the functional connectivity and the synchronization between rACC and BLA regions, but also enhanced the pain–related neural information flow from rACC to BLA.

4. Discussion

In this study, we provided several lines of evidence to show that chronic FS stress (CFSS) could result in an increased activity of rACC neuronal population and promote the functional connectivity and synchronization between rACC and BLA regions, and also, enhance the pain–related neural information flow from rACC to BLA, which likely underlie the pathogenesis of stress–induced hyperalgesia (SIH). First, we found that CFSS could indeed increase the pain sensitivity of rats in response to low intensity innoxious stimuli (LIS) and high intensity noxious stimuli (HNS) imposed upon the hindpaw, presenting a direct validation for SIH. Second, we discovered that CFSS not only induced an increased activity of rACC neuron population but also produced an augmented field potential power (FPP) of rACC LFP, especially in low frequency theta band as well as in high frequency low gamma band ranges, both at the baseline state and under LIS and HNS conditions. Third, by using a cross-correlation method and a partial directed coherence (PDC) algorithm to analyze the oscillating activity of rACC and BLA LFPs, we demonstrated that CFSS could substantially promote the synchronization between rACC and BLA regions, and also enhance the neural information flow from rACC to BLA.

Exposure to chronic or repeated stress can produce maladaptive neurobiological changes in pathways associated with pain processing, resulting in a stress–induced hyperalgesia (SIH) (Jennings et al., 2014). Stress can either suppress pain (stress–induced analgesia) or exacerbate it (SIH) depending on the nature, duration and intensity of the stressor (Olango and Finn, 2014). There are common mechanisms underlying the pathogenesis of SIH and the comorbidity of chronic pain and psychiatric disorders such as anxiety and depression. In our present study, we found that exposure of CFSS to rats indeed resulted in an increased pain sensitivity in response to LIS and HNS imposed upon the hindpaw, which may provide a direct validation for SIH, a common phenomenon also observed in human beings (Jennings et al., 2014).

The ACC plays a critical role in initiation, development, and maintenance of chronic pain (Wager et al., 2016; Yang et al., 2015). It also plays an important role in the perception of nociceptive information and associated emotional processing of pain (Chen et al., 2018b; Lee et al., 2017; Wager et al., 2016), and thus is considered as an important brain region for integrating the emotional components of pain (Blom et al., 2014). Accordantly, optogenetic stimulation of the ACC is sufficient to induce pain and pain-related anxiety and depressive-like behaviors in normal animals (Barthas et al., 2015), supporting the notion that the ACC may mediate the interaction between anxiety, depression and chronic pain (Koga et al., 2015; Zugaib et al., 2014). It has been reported that the rACC region may serve as a modulator for the affective behavior manifestations of visceral, motor and endocrine through projecting to the downstream brain regions involved in pain perception (Price, 2000; Schnitzler and Ploner, 2000). The spontaneous firing activity of rACC neurons correlates with increased visceral pain responses and also is associated with the affective aspects of pain (Wang et al., 2015; Xiao and Zhang, 2018). Several clinical and pre-clinical data have shown that abnormal activation of rACC neurons in stress–-related disorders and/or during stress states may increase nociception and augment the affective aspects of pain experience (Jennings et al., 2014; Xiao and Zhang, 2018). In line with these findings, we discovered that exposure of CFSS to rats not only induced an increased spontaneous activity of rACC neurons at the baseline state but also enhanced the rACC neuron activity in response to LIS and HNS, indicating that chronic stress may induce a sensitization of rACC neurons in rats.

Brain rhythmical oscillations in the low (delta, theta, and alpha) and high (beta and gamma) frequency ranges of electroencephalography are linked to broad varieties of perceptual, sensorimotor, and cognitive operations (Schroeder and Lakatos, 2009). For example, delta band oscillation is associated with compromised neuronal function (Steriade, 2006), alpha band oscillation mainly serves as a top-down controlled inhibitory mechanism (Knyazev, 2007), and theta band oscillation may promote neural plasticity (Masquelier et al., 2009) and participate in the process of information processing for touch and pain (Michail et al., 2016; Schulz et al., 2011). Theta oscillation also plays a crucial network-level role in hippocampal function, thus suppressing theta rhythm oscillation may impair learning and memory (McNaughton et al., 2006). In inflammatory rats, an increased activity of FPP was found in delta, theta, and alpha frequency bands in rACC LFP (Harris-Bozer and Peng, 2016). These findings support our understanding for the role of low-frequency oscillations in pain processing and SIH generating. On the other hand, high-frequency beta oscillation may be involved in the maintenance of the current sensorimotor or cognitive state, and the extraordinary enhancement of beta oscillation may result in an abnormal persistence of the current situation and a deterioration of flexible behaviors and cognitive controls (Engel and Fries, 2010), while gamma band oscillation may play an important role in selecting and integrating sensory-relevant information into a coherent perception (Herrmann et al., 2004), and participate in pain perception and abnormal pain memory (Cardoso-Cruz et al., 2013; Zhang et al., 2012). The FPP of gamma band oscillations was increased after noxious laser stimuli in healthy human beings (Liu et al., 2015; Tiemann et al., 2010) and animals (Wang et al., 2011; Wang et al., 2017; Wang et al., 2016). An increased gamma band oscillation was also observed in frontal-central region in subjects suffered from tonic muscle pain (Li et al., 2016) or tonic heat pain (Peng et al., 2014). In addition, the gamma frequency range can be further classified into low (or slow) gamma (31–70 Hz) and high (or fast) gamma (71–100 Hz) bands to indicate distinct network states with different functions of the brain activity (Zheng et al., 2015). Distinction between low- and high-frequency gamma bands is important for evaluating the effect of general anesthetics on brain electrical activity, and the attenuation and inter-regional desynchronization of high-frequency gamma oscillations appear to correlate with the loss of consciousness (Hudetz et al., 2011). Synchronization of neuronal activity in the visual cortex at low and high gamma band frequencies also has been associated with distinct visual processes (Oke et al., 2010). In support of these ideas, we found that the baseline FPP of rACC LFP, both in low frequency theta and alpha bands and in high frequency low gamma band ranges, was substantially increased in rats subjected to CFSS. Likewise, the activity of rACC FPP induced by LIS and HNS were also significantly increased in theta and low gamma frequency bands in CFSS-treated rats. These findings present solid evidence for our understanding that an increased synchronization of rACC neuronal activity, manifested by the augmentation of rACC FPP in theta and low gamma frequency bands, may play an important role in SIH processing.

Previously, we have reported that the amygdala is involved in CFSS–induced depressive-like behaviors and the exacerbation of neuropathic pain in rats (Chen et al., 2018a; Li et al., 2017), of which, the BLA and CeA are shown to play important roles in the integration of affective and sensory information including nociception (Li et al., 2017; Padival et al., 2013). Direct neuronal projections from ACC to BLA also participate in emotional functions such as fear learning (Allsop et al., 2018; Jhang et al., 2016). The association between rACC and amygdala was increased in a variety of neurological and psychiatric disorders including neuropathic pain (Cao et al., 2016), whereas disruption of synchronized theta oscillations in the ACC–BLA pathway was suggested contribute to the emotional and cognitive deficits in rats (Mu et al., 2015). In addition, cross-frequency coherence has functional significant in both information processing and detecting broad-range correlations of field potential oscillations and the synchronization among different brain regions (Benchenane et al., 2011; Buzsaki and Schomburg, 2015), thereby potentially reflecting the functional connectivity of these areas (Herrmann et al., 2004). It is known that the occurrence of negative lags at the coherence peak indicates that one brain region leads another brain region, and vice-versa, while the close to-zero lag means simultaneous activity between the two regions (Adhikari et al., 2010; Taghva et al., 2012). In this study, as analyzed for both LIS-evoked LFP and HNS-evoked LFP in rACC and BLA, we robustly observed an evident close to-zero lag appeared on the rACC–BLA correlation peak, suggesting a high synchronization between these two brain regions after exposure of CFSS to rats. Moreover, we found that the coherence coefficient between low and low, high and high, low and high frequency bands, as well as between theta and theta, low gamma and low gamma, theta and low gamma frequency bands, of both LIS-evoked LFP and HNS-evoked LFP in rACC and BLA, were significantly increased after stress in the CFSS-treated rats. Consistently, accumulative evidence has documented that painful laser stimuli can induce event-related theta (Mu et al., 2008) and gamma-band activity (Kim et al., 2015), and the amplitude of gamma power is positively increased coupling with the phase of theta oscillations in chronic inflammatory pain condition (Wang et al., 2016). The theta oscillation of baseline state relates to persistent pain (Fallon et al., 2018), while spontaneous gamma activity (Schulz et al., 2012) and functional connectivity (Fomberstein et al., 2013) are closely connected with the severity of chronic pain. In addition, the theta-gamma phase locking is weakened in depressive-like rats (Zheng and Zhang, 2013), while changes in theta (Taesler and Rose, 2016) and gamma (Leblanc et al., 2014) band power are covarying with subsequent pain perception, and the high activity levels of theta oscillations as well as the balancing and coupling between neural oscillations are also significantly correlated with pain relief (Huang et al., 2018). Together these data with our findings, we suggested that exposure of CFSS to rats may increase the functional connectivity and the synchronization between rACC and BLA regions, and subsequently participate in SIH processing.

To further determine the directionality of the neural information flow between rACC and BLA during SIH processing, we analyzed partial directed coherence (PDC) using the phase and power information of LFPs, to test the potential causal effects of these two brain regions (Li et al., 2018). We found that exposure of CFSS to rats could substantially increase the normalized PDC value of rACC–BLA pathway in theta band of HNS-induced LFP, indicating that chronic FS stress likely enhances the neural information flow from rACC to BLA, to mediate the CFSS–induced augmentation of pain sensitivity.

In conclusion, our present data suggest that exposure of chronic FS stress to rats increases rACC neuron activity, promotes the functional connectivity and synchronization between rACC and BLA regions, and also enhances the pain–related neural information flow from rACC to BLA, which likely underlies the pathogenesis of SIH. These findings extend the understanding of the brain mechanisms underlying SIH processing.

Declaration of interest

The authors declare that they have no competing financial interests to disclose.

Acknowledgments

This work was supported by the grants from the National Natural Science Foundation of China (81671085, 61527815, 81371237) and the National Basic Research Program of China (973 Program, 2013CB531905).

Appendix A. Supplementary data

Supplementary data to this article can be found online at https://doi.org/10.1016/j.expneurol.2018.12.009.

References

Adhikari, A., Sigurdsson, T., Topiwala, M.A., Gordon, J.A., 2010. Cross-correlation of instantaneous amplitudes of field potential oscillations: a straightforward method to estimate the directionality and lag between brain areas. J. Neurosci. Methods 191, 191–200.
Akechi, T., Okuyama, T., Uchida, M., Nakaguchi, T., Sugano, K., Kubota, Y., Ito, Y., Kizawa, Y., Komatsu, H., 2012. Clinical indicators of depression among ambulatory cancer patients undergoing chemotherapy. Jpn. J. Clin. Oncol. 42, 1175–1180.
Allsop, S.A., Wichmann, R., Mills, F., Burgos-Robles, A., Chang, C.-J., Felix-Ortiz, A.C., Vienne, A., Beyeler, A., Izadmehr, E.M., Glober, G., Cum, M.I., Stergiadou, J., Anandalingam, K.K., Farris, K., Namburi, P., Leppla, C.A., Weddington, J.C., Nieh, E.H., Smith, A.C., Ba, D., Brown, E.N., Tye, K.M., 2018. Corticoamygdala transfer of socially derived information gates observational learning. Cell 173, 1329–1342.
Barthas, F., Sellmeijer, J., Hugel, S., Waltisperger, E., Barrot, M., Yalcin, I., 2015. The anterior cingulate cortex is a critical hub for pain-induced depression. Biol. Psychiatry 77, 236–245.
Benchenane, K., Tiesinga, P.H., Battaglia, F.P., 2011. Oscillations in the prefrontal cortex: a gateway to memory and attention. Curr. Opin. Neurobiol. 21, 475–485.
Bianchi, R., Corsetti, G., Rodella, L., Tredici, G., Gioia, M., 1998. Supraspinal connections and termination patterns of the parabrachial complex determined by the biocytin anterograde tract-tracing technique in the rat. J. Anat. 193, 417–430.
Blom, S.M., Pfister, J.P., Santello, M., Senn, W., Nevian, T., 2014. Nerve injury-induced neuropathic pain causes disinhibition of the anterior cingulate cortex. J. Neurosci. 34, 5754–5764.
Bogdanova, O.V., Kanekar, S., D'Anci, K.E., Renshaw, P.F., 2013. Factors influencing behavior in the forced swim test. Physiol. Behav. 118, 227–239.
Buzsaki, G., Schomburg, E.W., 2015. What does gamma coherence tell us about inter-regional neural communication? Nat. Neurosci. 18, 484–489.
Cao, B., Wang, J., LiMu, Poon, Li, Y., 2016. Impairment of decision making associated with disruption of phase-locking in the anterior cingulate cortex in viscerally hypersensitive rats. Exp. Neurol. 286, 21–31.
Cardoso-Cruz, H., Sousa, M., Vieira, J.B., Lima, D., Galhardo, V., 2013. Prefrontal cortex and mediodorsal thalamus reduced connectivity is associated with spatial working memory impairment in rats with inflammatory pain. Pain 154, 2397–2406.
Chen, L., Li, S., Cai, J., Wei, T.J., Liu, L.Y., Zhao, H.Y., Liu, B.H., Jing, H.B., Jin, Z.R., Liu, M., Wan, Y., Xing, G.G., 2018a. Activation of CRF/CRFR1 signaling in the basolateral nucleus of the amygdala contributes to chronic forced swim-induced depressive-like behaviors in rats. Behav. Brain Res. 338, 134–142.
Chen, Z., Shen, X., Huang, Wu, Zhang, M., 2018b. Membrane potential synchrony of neurons in anterior cingulate cortex plays a pivotal role in generation of neuropathic pain. Sci. Rep. 8, 1691.
Clauss, J.A., Avery, S.N., VanDerKlok, R.M., Rogers, B.P., Cowan, R.L., Benningfield, M.M., Blackford, J.U., 2014. Neurocircuitry underlying risk and resilience to social anxiety disorder. Depression and anxiety 31, 822–833.
Engel, A.K., Fries, P., 2010. Beta-band oscillations–signalling the status quo? Curr. Opin. Neurobiol. 20, 156–165.
Fallon, N., Chiu, Y., Nurmikko, T., Stancak, A., 2018. Altered theta oscillations in resting EEG of fibromyalgia syndrome patients. Eur. J. Pain 22, 49–57.
Fomberstein, K., Qadri, S., Ramani, R., 2013. Functional MRI and pain. Curr. Opin. Anaesthesiol. 26, 588–593.
Gerrits, M.M., van Oppen, P., van Marwijk, H.W., Penninx, B.W., van der Horst, H.E., 2014. Pain and the onset of depressive and anxiety disorders. Pain 155, 53–59.
Goncalves, L., Silva, R., Pinto-Ribeiro, F., Pego, J.M., Bessa, J.M., Pertovaara, A., Sousa, N., Almeida, A., 2008. Neuropathic pain is associated with depressive behaviour and induces neuroplasticity in the amygdala of the rat. Exp. Neurol. 213, 48–56.
Guo, B., Wang, J., Yao, H., Ren, K., Chen, J., Yang, J., Cai, G., Liu, H., Fan, Y., Wang, W., Wu, S., 2018. Chronic Inflammatory Pain Impairs mGluR5-Mediated Depolarization-Induced suppression of Excitation in the Anterior Cingulate Cortex. Cereb. Cortex 28, 2118–2130.
Harris, A.Z., Gordon, J.A., 2015. Long-range neural synchrony in behavior. Annu. Rev. Neurosci. 38, 171–194.
Harris-Bozer, A.L., Peng, Y.B., 2016. Inflammatory pain by carrageenan recruits low-frequency local field potential changes in the anterior cingulate cortex. Neurosci. Lett. 632, 8–14.
Herrmann, C.S., Munk, M.H., Engel, A.K., 2004. Cognitive functions of gamma-band activity: memory match and utilization. Trends Cogn. Sci. 8, 347–355.
Huang, Y., Green, A.L., Hyam, J., Fitzgerald, J., Aziz, T.Z., Wang, S., 2018. Oscillatory neural representations in the sensory thalamus predict neuropathic pain relief by deep brain stimulation. Neurobiol. Dis. 109, 117–126.
Hudetz, A.G., Vizuete, J.A., Pillay, S., 2011. Differential effects of isoflurane on high-frequency and low-frequency gamma oscillations in the cerebral cortex and hippocampus in freely moving rats. Anesthesiology 114, 588–595.
Jennings, E.M., Okine, B.N., Roche, M., Finn, D.P., 2014. Stress-induced hyperalgesia. Prog. Neurobiol. 121, 1–18.
Jensen, K.B., Berna, C., Loggia, M.L., Wasan, A.D., Edwards, R.R., Gollub, R.L., 2012. The use of functional neuroimaging to evaluate psychological and other non-pharmacological treatments for clinical pain. Neurosci. Lett. 520, 156–164.
Jhang, J., Lee, H., Kang, M.S., Lee, H.-S., Park, H., Han, J.-H., 2016. Anterior cingulate cortex and its input to the basolateral amygdala control innate fear response. Nat. Commun. 9, 1–16.
Kim, J.H., Chien, J.H., Liu, C.C., Lenz, F.A., 2015. Painful cutaneous laser stimuli induce event-related gamma-band activity in the lateral thalamus of humans. J. Neurophysiol. 113, 1564–1573.
Knyazev, G.G., 2007. Motivation, emotion, and their inhibitory control mirrored in brain oscillations. Neurosci. Biobehav. Rev. 31, 377–395.
Koga, K., Descalzi, G., Chen, T., Ko, H.G., Lu, J., Li, S., Son, J., Kim, T., Kwak, C., Huganir, R.L., Zhao, M.G., Kaang, B.K., Collingridge, G.L., Zhuo, M., 2015. Coexistence of two forms of LTP in ACC provides a synaptic mechanism for the interactions between anxiety and chronic pain. Neuron 85, 377–389.
Leblanc, B.W., Lii, T.R., Silverman, A.E., Alleyne, R.T., Saab, C.Y., 2014. Cortical theta is

increased while thalamocortical coherence is decreased in rat models of acute and chronic pain. Pain 155, 773–782.
Lee, P.S., Low, I., Chen, Y.S., Tu, C.H., Chao, H.T., Hsieh, J.C., Chen, L.F., 2017. Encoding of menstrual pain experience with theta oscillations in women with primary dysmenorrhea. Sci. Rep. 7, 15977.
Li, J.X., 2015. Pain and depression comorbidity: a preclinical perspective. Behav. Brain Res. 276, 92–98.
Li, L., Liu, X., Cai, C., Yang, Y., Li, D., Xiao, L., Xiong, D., Hu, L., Qiu, Y., 2016. Changes of gamma-band oscillatory activity to tonic muscle pain. Neurosci. Lett. 627, 126–131.
Li, M.J., Liu, L.Y., Chen, L., Cai, J., Wan, Y., Xing, G.G., 2017. Chronic stress exacerbates neuropathic pain via the integration of stress-affect-related information with nociceptive information in the central nucleus of the amygdala. Pain 158, 717–739.
Li, P., Huang, X., Zhu, X., Liu, H., Zhou, W., Yao, D., Xu, P., 2018. Lp (p < /= 1) norm partial directed coherence for directed network analysis of scalp EEGs. Brain Topogr. 31, 738–752.
Liu, C.C., Chien, J.H., Chang, Y.W., Kim, J.H., Anderson, W.S., Lenz, F.A., 2015. Functional role of induced gamma oscillatory responses in processing noxious and innocuous sensory events in humans. Neuroscience 310, 389–400.
Masquelier, T., Hugues, E., Deco, G., Thorpe, S.J., 2009. Oscillations, phase-of-firing coding, and spike timing-dependent plasticity: an efficient learning scheme. J. Neurosci. 29, 13484–13493.
Matyas, F., Lee, J., Shin, H.S., Acsady, L., 2014. The fear circuit of the mouse forebrain: connections between the mediodorsal thalamus, frontal cortices and basolateral amygdala. Eur. J. Neurosci. 39, 1810–1823.
McNaughton, N., Ruan, M., Woodnorth, M.A., 2006. Restoring theta-like rhythmicity in rats restores initial learning in the Morris water maze. Hippocampus 16, 1102–1110.
Michail, G., Dresel, C., Witkovsky, V., Stankewitz, A., Schulz, E., 2016. Neuronal oscillations in various frequency bands differ between pain and touch. Front. Hum. Neurosci. 10, 182.
Mu, Y., Fan, Y., Mao, L., Han, S., 2008. Event-related theta and alpha oscillations mediate empathy for pain. Brain Res. 1234, 128–136.
Mu, L., Wang, J., Cao, B., Jelfs, B., Chan, R.H., Xu, X., Hasan, M., Zhang, X., Li, Y., 2015. Impairment of cognitive function by chemotherapy: association with the disruption of phase-locking and synchronization in anterior cingulate cortex. Mol. Brain 8, 32.
Oke, O.O., Magony, A., Anver, H., Ward, P.D., Jiruska, P., Jefferys, J.G., Vreugdenhil, M., 2010. High-frequency gamma oscillations coexist with low-frequency gamma oscillations in the rat visual cortex in vitro. Eur. J. Neurosci. 31, 1435–1445.
Olango, W.M., Finn, D.P., 2014. Neurobiology of stress-induced hyperalgesia. Curr. Top. Behav. Neurosci. 20, 251–280.
Padival, M., Quinette, D., Rosenkranz, J.A., 2013. Effects of repeated stress on excitatory drive of basal amygdala neurons in vivo. Neuropsychopharmacology 38, 1748–1762.
Paxinos, G., Watson, C.R., 2005. The Rat Brain in Stereotaxic Coordinates, 5th ed. Elsevier Academic Press, San Diego.
Peng, W., Hu, L., Zhang, Z., Hu, Y., 2014. Changes of spontaneous oscillatory activity to tonic heat pain. PLoS One 9, e91052.
Price, D.D., 2000. Psychological and neural mechanisms of the affective dimension of pain. Science 288, 1769–1772.
Schnitzler, A., Ploner, M., 2000. Neurophysiology and functional neuroanatomy of pain perception. J. Clin. Neurophysiol. 17, 592–603.
Schroeder, C.E., Lakatos, P., 2009. Low-frequency neuronal oscillations as instruments of sensory selection. Trends Neurosci. 32, 9–18.
Schulz, E., Tiemann, L., Schuster, T., Gross, J., Ploner, M., 2011. Neurophysiological coding of traits and states in the perception of pain. Cereb. Cortex 21, 2408–2414.
Schulz, E., Tiemann, L., Witkovsky, V., Schmidt, P., Ploner, M., 2012. Gamma Oscillations are involved in the sensorimotor transformation of pain. J. Neurophysiol. 108, 1025–1031.
Seno, M.D.J., Assis, D.V., Gouveia, F., Antunes, G.F., Kuroki, M., Oliveira, C.C., Santos, L.C.T., Pagano, R.L., Martinez, R.C.R., 2018. The critical role of amygdala subnuclei in nociceptive and depressive-like behaviors in peripheral neuropathy. Sci. Rep. 8, 13608.
Sharp, B.M., 2017. Basolateral amygdala and stress-induced hyperexcitability affect motivated behaviors and addiction. Transl. Psychiatry 7, e1194.
Shinozaki, R., Hojo, Y., Mukai, H., Hashizume, M., Murakoshi, T., 2016. Kainate-induced network activity in the anterior cingulate cortex. Neuroscience 325, 20–29.
Shishkina, G.T., Kalinina, T.S., Bulygina, V.V., Lanshakov, D.A., Babluk, E.V., Dygalo, N.N., 2015. Anti-Apoptotic Protein Bcl-xL Expression in the Midbrain Raphe Region is Sensitive to stress and Glucocorticoids. PLoS One 10, e0143978.
Steriade, M., 2006. Grouping of brain rhythms in corticothalamic systems. Neuroscience 137, 1087–1106.
Strobel, C., Hunt, S., Sullivan, R., Sun, J., Sah, P., 2014. Emotional regulation of pain: the role of noradrenaline in the amygdala. Sci. China Life Sci. 57, 384–390.
Suarez-Roca, H., Leal, L., Silva, J.A., Pinerua-Shuhaibar, L., Quintero, L., 2008. Reduced GABA neurotransmission underlies hyperalgesia induced by repeated forced swimming stress. Behav. Brain Res. 189, 159–169.
Taesler, P., Rose, M., 2016. Prestimulus theta oscillations and connectivity modulate pain perception. J. Neurosci. 36, 5026–5033.
Taghva, A., Song, D., Hampson, R.E., Deadwyler, S.A., Berger, T.W., 2012. Determination of relevant neuron-neuron connections for neural prosthetics using time-delayed mutual information: tutorial and preliminary results. World Neurosurgery 78, 618–630.
Tiemann, L., Schulz, E., Gross, J., Ploner, M., 2010. Gamma oscillations as a neuronal correlate of the attentional effects of pain. Pain 150, 302–308.
Wager, T.D., Atlas, L.Y., Botvinick, M.M., Chang, L.J., Coghill, R.C., Davis, K.D., Iannetti, G.D., Poldrack, R.A., Shackman, A.J., Yarkoni, T., 2016. Pain in the ACC. Proc. Natl. Acad. Sci. U. S. A. 113, E2474–E2475.
Wang, J., Li, D., Li, X., Liu, F.Y., Xing, G.G., Cai, J., Wan, Y., 2011. Phase-amplitude coupling between theta and gamma oscillations during nociception in rat electroencephalography. Neurosci. Lett. 499, 84–87.
Wang, J., Cao, B., Yu, T.R., Jelfs, B., Yan, J., Chan, R.H., Li, Y., 2015. Theta-frequency phase-locking of single anterior cingulate cortex neurons and synchronization with the medial thalamus are modulated by visceral noxious stimulation in rats. Neuroscience 298, 200–210.
Wang, J., Wang, J., Xing, G.G., Li, X., Wan, Y., 2016. Enhanced gamma oscillatory activity in rats with chronic inflammatory pain. Front. Neurosci. 10, 489.
Wang, J., Wang, J., Wan, Y., Li, X., 2017. The frontal area with higher frequency response is the principal feature of laser-evoked potentials in rats with chronic inflammatory pain: a parallel factor analysis study. Front. Neurol. 8, 155.
Xiao, X., Zhang, Y.Q., 2018. A new perspective on the anterior cingulate cortex and affective pain. Neurosci. Biobehav. Rev. 90, 200–211.
Yang, J.X., Hua, L., Li, Y.Q., Jiang, Y.Y., Han, D., Liu, H., Tang, Q.Q., Yang, X.N., Yin, C., Hao, L.Y., Yu, L., Wu, P., Shao, C.J., Ding, H.L., Zhang, Y.M., Cao, J.L., 2015. Caveolin-1 in the anterior cingulate cortex modulates chronic neuropathic pain via regulation of NMDA receptor 2B subunit. J. Neurosci. 35, 36–52.
Yankelevitch-Yahav, R., Franko, M., Huly, A., Doron, R., 2015. The forced swim test as a model of depressive-like behavior. J. Visual. Exp. 1–7.
Yoshimura, S., Okamoto, Y., Onoda, K., Matsunaga, M., Ueda, K., Suzuki, S., 2010. Rostral anterior cingulate cortex activity mediates the relationship between the depressive symptoms and the medial prefrontal cortex activity. J. Affect. Disord. 122, 76–85.
Zhang, Z.G., Hu, L., Hung, Y.S., Mouraux, A., Iannetti, G.D., 2012. Gamma-band oscillations in the primary somatosensory cortex–a direct and obligatory correlate of subjective pain intensity. J. Neurosci. 32, 7429–7438.
Zheng, C., Zhang, T., 2013. Alteration of phase-phase coupling between theta and gamma rhythms in a depression-model of rats. Cogn. Neurodyn. 7, 167–172.
Zheng, C., Bieri, K.W., Trettel, S.G., Colgin, L.L., 2015. The relationship between gamma frequency and running speed differs for slow and fast gamma rhythms in freely behaving rats. Hippocampus 25, 924–938.
Zugaib, J., Coutinho, M.R., Ferreira, M.D., Menescal-de-Oliveira, L., 2014. Glutamate/GABA balance in ACC modulates the nociceptive responses of vocalization: an expression of affective-motivational component of pain in Guinea pigs. Physiol. Behav. 126, 8–14.